Recent Developments and Trends in Redox Flow Batteries

Liang Su, Jeffrey A. Kowalski, Kyler J. Carroll and Fikile R. Brushett

1 Introduction

A major challenge of the 21st century is the development of efficient and sustainable means of energy conversion, distribution, and storage on a global scale. Presently, fossil fuel technologies make up the backbone of our energy economy, notably transportation and bulk generation for electrification. The International Energy Agency (IEA) reported that, in 2012, of the total energy consumed worldwide, around 70.8 % was derived from fossil fuel sources (oil, natural gas, coal, etc.), with the majority of energy consumption and demand growth coming from developing nations [1]. In the United States, the 2011 Energy Information Administration (EIA) annual review reported that around 78 % of the total energy consumed was derived from fossil fuel sources (i.e., oil, coal, and natural gas) and the two largest consumption sectors are electricity (38 %) and transportation (27 %), both of which are dominated by fossil fuel sources [2, 3]. However, in the future, this energy mix will not be feasible [4]. Rising population and continuing economic growth in the developing world are projected to double global energy consumption by 2050 [3]. Non-renewable fossil fuel reserves, which took millennia to accumulate, are finite and rapidly disappearing. Moreover, the continued and increasing generation of anthropogenic carbon dioxide (CO_2) from fossil fuel combustion will likely have negative implications for the global climate [5]. Analysis by the Intergovernmental Panel on Climate Change (IPCC) indicated that to stabilize the atmospheric concentration of CO_2 at 350–400 ppm (near its current level), global CO_2 emissions would need to be tapered by 2050 to a level of 20–50 % of the 2000 emissions [6]. Thus a tremendous need exists for scientific and technological advances to address these grand challenges, sparking worldwide

L. Su · J.A. Kowalski · K.J. Carroll · F.R. Brushett (✉)
Department of Chemical Engineering, Massachusetts Institute of Technology, Cambridge, MA 02139, USA
e-mail: brushett@mit.edu

Z. Zhang and S.S. Zhang (eds.), *Rechargeable Batteries*,
Green Energy and Technology, DOI 10.1007/978-3-319-15458-9_24

investment in low-carbon/carbon-neutral power generation, carbon capture and storage, and system-wide energy efficiency [7].

Stationary energy storage systems (ESS) will play a pivotal role in the widespread integration of renewable, non-dispatchable energy sources (e.g., solar photovoltaic (PV), wind) and in the improvement of energy efficiency of the electric grid [8, 9]. Indeed, increased energy storage assets can enhance energy security, reduce carbon emissions, and introduce new revenue streams for a range of stakeholders [10, 11]. In cases where no transmission or distribution constraints exist, grid-connected ESS are not required to be co-located with the energy source, providing the flexibility to optimize storage performance characteristics and minimize costs. Where constraints exist (e.g., developing economies, island nations), coupling energy storage with local generation resources (e.g., solar PV, fuel cells, micro-turbines) can enable the development of robust micro-grids. Services provided by ESS and their remuneration create the incentive for adopting energy storage. These services can be broadly classified as bulk energy, ancillary, transmission and distribution (T&D), renewables integration, and customer energy management (Table 1) [12, 13]. However, despite this promise, only $\sim$ 2.5 % of total electric production in the US relies on grid energy storage with the principal barrier to widespread installation being the system cost [14]. Therefore, the development of cost competitive energy storage technologies with validated reliability and safety is of paramount importance to the continued evolution of the electric power sector in the US and worldwide.

While a range of ESS options exist to meet the aforementioned services, no single technology is suitable for all applications. Present storage technologies vary in their performance characteristics, level of technological maturity, and, most importantly, cost. The applicability of different technologies based on their associated attributes is shown in Fig. 1, an adaptation from a recent Sandia National Laboratory report [15]. The storage technology comparison shown divides the applications roughly into three broad segments based on the discharge time and system power requirements: uninterruptible power supply, T&D grid support-load shifting, and bulk management. Both cost and bulk-storage-relevant attributes have resulted in pumped hydroelectric storage (pumped hydro) being responsible for over 97 % of the worldwide energy storage capacity (ca. 127 GW) [16]. Pumped hydro however suffers from constraints arising from geographical settings, licensing, environmental regulations, and uncertainty in long-term electric markets [10, 17]. Though they presently constitute a significantly smaller installed capacity (ca. 400 MW), electrochemical energy storage technologies have a number of desirable characteristics including high power/energy density, high round-trip efficiency, rapid response time, and terrain-independence. However, the economics of grid storage are challenging. In a 2013 report, the United States Department of Energy (DOE) has outlined a near-term system capital cost goal of $250/kWh for grid storage systems with a long term reduction to $150/kWh [10]. Other DOE programs have proposed more aggressive cost targets. For example, the Advanced Research Projects Agency-Energy (ARPA-E) Grid-Scale Rampable Intermittent Dispatchable Storage (GRIDS) program has set a target of less than $100/kWh for

Table 1 Key characteristics of storage systems for selected energy services adapted from Ref. [13]

Services	Size (MW)	Discharge duration	Cycles (typical)	Response time	Output (electricity 'e', thermal 't')
Bulk energy services					
Seasonal storage	500–2000	d–mo	1–5/y	d	e, t
Arbitrage	100–2000	8–24 h	0.25–1/d	>1 h	e
Ancillary services					
Frequency regulation	1–2000	1–15 min	20–40/d	1 min	e
Load following	1–2000	15 min–1 d	1–29/d	<15 min	e, t
Voltage support	1–40	1–60 s	10–100/d	0.001–1 s	e
Black start	0.1–400	1–4 h	<1/y	<1 h	e
Spinning reserve	10–2000	15 min–2 h	0.5–2/d	<15 min	e
Non-spinning reserve	10–2000	15 min–2 h	0.5–2/d	>15 min	e
Transmission and distribution infrastructure services					
Transmission and distribution congestion relief	10–500	2–4 h	0.14–1.25/d	>1 h	e, t
Transmission and distribution investment deferral	1–500	2–5 h	0.75–1.25/d	>1 h	e, t
Renewable and other integration services					
Variable Supply Resource Integration	1–400	1 min–h	0.5–2/d	<15 min	e, t
Waste Heat Utilization	1–10	1–24 h	1–20/d	<10 min	t
Combined Heat and Power	1–5	min–h	1–10/d	<15 min	t
Customer energy management services					
Demand shifting and peak reduction	0.001–1	min–h	1–29/d	<15 min	e, t
Off-grid	0.001–	3–5 h	0.75–1.5/d	<1 h	e, t

new storage technologies [18]. Further, the Joint Center for Energy Storage Research (JCESR), a DOE-funded Energy Innovation Hub, aims to develop battery prototypes that, when scaled to manufacturing, are projected to reach battery price levels to enable widespread market adoption (e.g., $100 per useable kWh) [19]. These stringent targets reflect the low cost of electricity in the United States but market penetration may be realized in global regions with higher electricity costs (e.g., Europe, Japan [1]) or through niche applications where higher system costs can be offset by the value of provided services.

Redox flow batteries (RFBs) have attracted considerable academic and industrial interest based on their favorable combination of performance, cost, and safety. Over the past few years, several comprehensive reviews have been published on RFBs

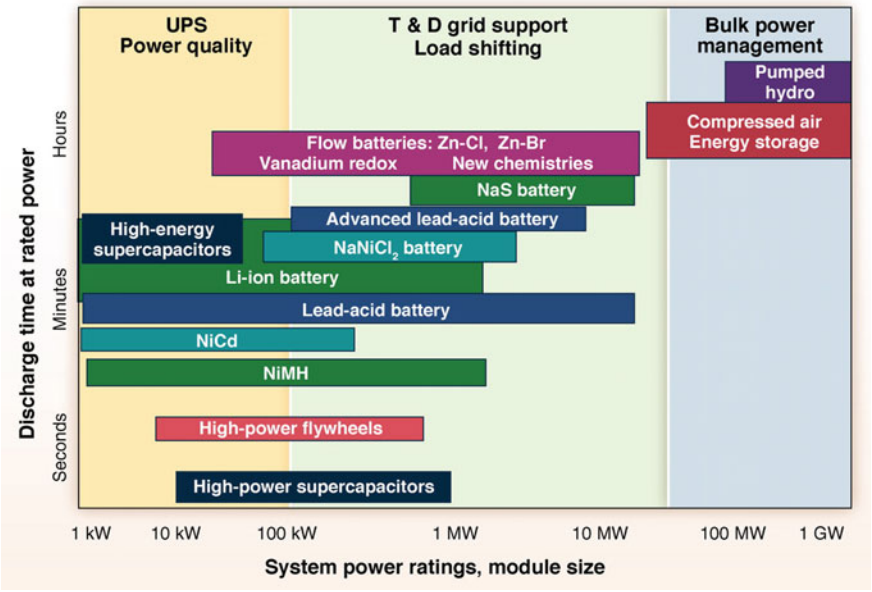

Fig. 1 Comparison of select storage technologies and associated addressable services broadly divided into three categories: uninterruptible power supply (UPS)-power quality, transmission and distribution (T&D) grid support-load shifting, and bulk power management. When roughly compared to Table 1, UPS-power quality is comparable to customer energy management services, T&D grid support-load shifting to ancillary services, T&D infrastructure services, renewable and other integration services, while bulk power management can be related to bulk energy services. Figure adapted from Ref. [15]. Reproduced with permission. Copyright 2010 Electric Power Research Institute

with detailed assessments of individual components (i.e., membranes [20–22] and electrodes/bipolar plates [23–25]) and of utility for stationary ESS applications [26–31]. For the sake of completeness, we will briefly review several topics covered in previous literature and, where appropriate, we will highlight in-depth reports for the interested reader. However, our goal is to discuss emerging, potentially transformative, strategies for enhancing RFB technologies through molecular design, electrolyte development, and cell-level engineering. In particular, we will survey the non-aqueous RFB literature which, to date, has been underrepresented in critical reviews. To this end, following a short overview of RFB basics and key performance metrics (Sect. 2), we highlight recent advances in redox active materials for aqueous and non-aqueous RFBs (Sect. 3) and new cell configurations to enhance common chemistries and enable the emerging redox couples and flowable formulations (Sect. 4). Finally, we conclude with future research directions and key challenges for RFB technologies (Sect. 5).

2 Overview of Redox Flow Batteries

A redox flow battery (RFB) is a rechargeable electrochemical device that utilizes the reversible redox reactions of two soluble electroactive species for energy storage. Figure 2 shows a simplified schematic of a flow battery. The system includes electrochemical reactors, storage vessels, circulation pumps, a heat exchanger, and power conditioning equipment. The positive and negative electrolytes (also referred to as the catholyte and anolyte) are fed to one or more electrochemical reactors, where the active species are oxidized or reduced to alternately charge or discharge the battery. Within an electrochemical cell, each electrolyte reacts on the corresponding positive or negative electrodes (also referred to as the cathode or anode), which are separated by either an ion-selective membrane or a nanoporous separator. These generic reactions are shown below (assuming a 1-electron transfer process):

Positive electrode:	$X^{n+} + e^- \rightleftharpoons X^{(n-1)+}$	E_1^0
Negative electrode:	$Y^{m+} + e^- \rightleftharpoons Y^{(m-1)+}$	E_2^0
Total reaction:	$X^{n+} + Y^{(m-1)-} \rightleftharpoons X^{(n-1)+} + Y^{m+}$	$E_{cell} = E_1^0 - E_2^0$

As compared to enclosed batteries, RFB architecture has several compelling features including:

- Independent power (W) and energy (Wh) due to separate tank and electroreactor configurations, which enables modular flexibility.
- Long life cycle with deep charge capabilities as storage is based on facile solution-phase redox reactions where the electrodes serve as a source or sink of electrons. Indeed, Skyllas-Kazacos et al. reported that durability generally exceeds 5000 deep cycles for flow batteries [31].
- Superior safety as reactants are contained in physically separated tanks with a relatively small volume in close proximity within the reactor stack.

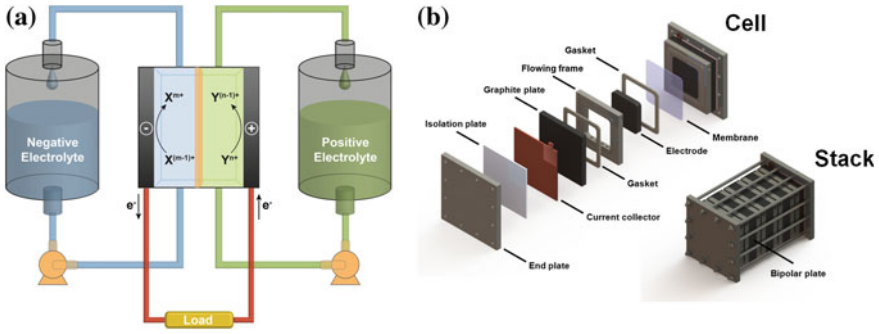

Fig. 2 **a** Schematic of a redox-flow cell (discharge mode). **b** Exploded view of components in a redox flow cell and an assembled redox flow battery with 4 stacked cells

- Simplified manufacturing and lower cell-to-cell variability due to simple electrode and stack construction. Further, replacement costs are likely to be lower.
- High active-to-inactive materials ratios are possible, especially for long duration storage where the battery cost asymptotically approaches the cost of redox solutions.

However, these advantages must be balanced against low energy density and increased system complexity. The energy densities of common aqueous flow systems, such as all-vanadium redox (VRB), are lower than those of enclosed batteries such as lead-acid and lithium-ion. Fortunately, this deficiency can be tolerated in many stationary applications. Flow battery systems require pumps to circulate the electrolytes, resulting in parasitic losses and complicating independent operation on the grid. Shunt currents between electrochemical cells within the stack also lead to efficiency losses. In this chapter, we will not contemplate these system-level considerations but direct the interested reader to reference [32] for the estimation of system efficiency in the presence of shunt current and pumping loss.

At present, RFBs are broadly considered too expensive for widespread deployment. While materials cost reductions can be expected through manufacturing scale and learning by doing, and additional contributions to price will decrease through competition and volume, new redox couples, electrolytes, and reactor configurations are likely needed to meet the DOE cost targets. As battery cost ($/kWh) are proportional to materials costs ($/kg) and inversely proportional to materials requirements (kWh/kg), two approaches can be taken to lower the system cost: cheaper storage materials and higher energy density (less material required). As we hope to highlight in this chapter, both of these avenues are being pursued by the research community.

3 Redox Active Compounds for Flow Cells

A wide range of electroactive materials have been investigated for use in RFBs. These materials can be broadly classified as inorganic compounds, which are far more prevalent at this point, and organic compounds, which are emergent. Moreover, their performance and durability have been evaluated in aqueous and non-aqueous electrolytes. In this section we highlight both select common and newly-identified redox couples and the resulting cell chemistries. While this treatment is representative rather than exhaustive, the ideal redox couple should be cost-effective and have the following properties: excellent reversibility and stability (both chemical and electrochemical), fast kinetics and mass transfer, and high solubility in relevant electrolytes. Note that only solution-phase redox reactions are discussed in this section. Dissolution/deposition reactions are introduced in Sect. 4.

3.1 Redox Active Compounds in Aqueous Flow Cells

3.1.1 Inorganic Redox Active Compounds

The application of inorganic electroactive compounds in aqueous RFBs have been the subject of the vast majority of the literature to date. Table 2 summarizes the standard electrode potentials of common redox couples while Table 3 highlights prominent cell chemistries based on combinations of these redox couples. Of these chemistries, iron–chromium (ICB) [33], polysulfide–bromide (PSB) [14], and all-vanadium (VRB) [31] systems have yielded industry-level demonstrations (order of 100 kW–10 MW). Below, these RFB chemistries are introduced in some detail with key advantages, disadvantages, and challenges highlighted.

Iron–Chromium Redox Flow Batteries

As the first modern RFB, the Fe–Cr system was proposed by NASA in 1973 and triggered considerable research activity on electrodes, membranes, and catalysts for optimizing performance and durability throughout the 1980s [43]. Furthermore, a 1 kW/13 kWh ICB system with 8 × 39-cell stacks was prototyped as the energy

Table 2 Electrochemical series for redox flow batteries [34]

Electrode reaction	E^0 (V)
$Li^+ + e^- \rightleftharpoons Li$	−3.040
$2H_2O + 2e^- \rightleftharpoons H_2 + 2OH^-$	−0.828
$Zn^{2+} + 2e^- \rightleftharpoons Zn$	−0.762
$Cr^{3+} + e^- \rightleftharpoons Cr^{2+}$	−0.407
$S_4^{2-} + 2e^- \rightleftharpoons 2S_2^{2-}$	−0.265
$V^{3+} + e^- \rightleftharpoons V^{2+}$	−0.255
$Pb^{2+} + 2e^- \rightleftharpoons Pb$	−0.126
$TiOH^{3+} + H^+ + 2e^- \rightleftharpoons Ti^{3+} + H_2O$	−0.055
$2H^+ + 2e^- \rightleftharpoons H_2$	0.000
$O_2 + 2H_2O + 4e^- \rightleftharpoons 4OH^-$	0.401
$I_3^- + 2e^- \rightleftharpoons 3I^-$	0.536
$Fe^{3+} + e^- \rightleftharpoons Fe^{2+}$	0.771
$VO_2^+ + 2H^+ + e^- \rightleftharpoons VO^{2+} + H_2O$	0.991
$Br_2 + 2e^- \rightleftharpoons 2Br^-$	1.807
$O_2 + 4H^+ + 4e^- \rightleftharpoons 2H_2O$	1.229
$PbO_2 + 4H^+ + 2e^- \rightleftharpoons Pb^{2+} + 2H_2O$	1.455
$Mn^{3+} + e^- \rightleftharpoons Mn^{2+}$	1.542
$Ce^{4+} + e^- \rightleftharpoons Ce^{3+}$	1.720

Here, E^0 represents the standard electrode potential

Table 3 Summary of major aqueous redox flow battery chemistries

Chemistry	Cell voltage (V)	Electrolyte (positive/negative)	Current density (mA/cm^2)	Efficiency	Reference
Fe/Ti	0.826	1 M $FeCl_3$ + 0.5 M HCl	≤25	CE ≈ 100 %	[35]
		1 M $TiCl_3$ + 6 M HCl		EE = 40 %	
Fe/V	1.026	1.25 M $FeCl_2$ + 1.25 M VCl_3 + 2.3 M HCl	50	CE = 97 %	[36]
		1.25 M $FeCl_2$ + 1.25 M VCl_3 + 2.3 M HCl		EE = 78 %	
Fe/Cr	1.178	1.25 M $FeCl_2$ + 2.3 M HCl + 1.25 M $CrCl_3$	40	CE = 97 %	[37]
		1.25 M $FeCl_2$ + 2.3 M HCl + 1.25 M $CrCl_3$		EE = 73 %	
VRB	1.246	1.5 M $VOSO_4$ + 2 M H_2SO_4	40	CE = 90 %	[38]
		1.5 M $VOSO_4$ + 2 M H_2SO_4		EE = 73 %	
Bromide/polysulfide	1.352	4.0 M NaBr	40	EE = 64 %	[39]
		1.3 M Na_2S_4			
Polyhalide/V	~1.43	1 M NaBr + 1 M HCl	20	CE = 83 %	[40]
		1 M VCl_3 + 1.5 M HCl		EE = 66 %	
Mn/V	1.797	0.3 M Mn(II) + 5 M H_2SO_4	20	CE = 69 %	[41]
		0.3 M V(III) + 5 M H_2SO_4		EE = 63 %	
Ce/V	1.975	0.5 M Ce(III) + 1 M H_2SO_4	22	CE = 87 %	[42]
		0.5 M V(III) + 1 M H_2SO_4			

Here, CE and EE represent coulombic efficiency and energy efficiency, respectively

storage device for a photovoltaic array in the early 1980s [44]. The electrode reactions are[1]:

$$\begin{aligned}
&\text{Positive electrode:} && Fe^{3+} + e^- \rightleftharpoons Fe^{2+} && E^0 = 0.771\,V\\
&\text{Negative electrode:} && Cr^{3+} + e^- \rightleftharpoons Cr^{2+} && E^0 = -0.407\,V\\
&\text{Total reaction:} && Fe^{3+} + Cr^{2+} \rightleftharpoons Fe^{2+} + Cr^{3+} && E = 1.178\,V
\end{aligned}$$

Hydrochloric acid and an cation or anion-selective membrane are commonly employed in the system. While the ferrous/ferric (Fe^{2+}/Fe^{3+}) redox couple demonstrates facile kinetics on carbonaceous surfaces, the kinetics of the chromous/chromic (Cr^{2+}/Cr^{3+}) couple are fairly sluggish, requiring a relatively high overpotential to drive the reaction. Thus, the hydrogen evolution reaction (HER) inevitably becomes a concern at these low potentials, resulting in the parasitic losses on the negative electrode. A gold-lead bimetallic electrocatalyst has been shown to effectively mitigate the problem as lead suppresses HER while gold catalyzes the redox reaction of Cr^{2+}/Cr^{3+} [44]. However, the incorporation of gold is undesirable as it dramatically

[1]All electrode potential values are referenced to the standard hydrogen electrode unless otherwise stated.

increases the capital cost. Moreover, for these systems, rebalancing the system due to side reactions and active species crossover (through the membrane) is necessary for long-term use, which adds to the overall operating expenses.

Polysulfide-Bromide Redox Flow Batteries

The PSB is an attractive chemistry due to the low cost, high abundance, and high solubility of both polysulfide and bromine in aqueous electrolytes. Considered applicable in MW/MWh class installations, this chemistry has been extensively studied since the earlier 1990s with several large-scale demonstration undertaken by various companies (e.g., Regenesys Technology) [14]. The electrode reactions are:

Positive electrode:	$Br_3^- + 2e^- \rightleftharpoons 3Br^-$	$E^0 = +1.087\,V$
Negative electrode:	$S_4^{2-} + 2e^- \rightleftharpoons 2S_2^{2-}$	$E^0 = -0.265\,V$
Total reaction:	$Br_3^- + 2S_2^{2-} \rightleftharpoons 3Br^- + S_4^{2-}$	$E = 1.352\,V$

A cation exchange membrane is typically used with a sodium ion shuttling between the positive and negative electrolytes containing NaBr and Na_2S_4, respectively. Nickel [45] and cobalt [39] have been found to catalyze the negative electrode reaction. Further, the use of activated carbon/polyolefin composite electrodes has been shown to increase charging voltages, from 1.7 to 2.1 V, due to bromine adsorption [31]. However, as with ICBs, species crossover over the operating life dramatically decreases the efficiency and capacity of the cell. Moreover, side reactions may lead to the formation of toxic gases (i.e., Br_2, H_2S) and insoluble insulating precipitants. Therefore, the system requires stringent maintenance to separate the electrolyte and to recover the reactants, which substantially increases the operating cost. Despite the favorable kinetics, the mass transfer overpotential on the positive electrode limits the discharge performance of the battery [46]. Scamman and coworkers developed a numerical model for PSBs, and showed that there would still be a net loss for arbitrage applications even if operated under optimum conditions. However, if the total capital cost were reduced by 20–30 % or the buy and sell price difference for electrical energy were increased, the system could become economically feasible [47].

All Vanadium Redox Flow Batteries

As arguably the most well-known RFB chemistry, VRBs take advantage of the four oxidation states of vanadium within the stability window of water. This enables operation with the same element as an electroactive species as both negative and positive electrolytes and limits concerns about solution crossover and the associated permanent deleterious effects (e.g., capacity fade, irreversible side reactions). Since the initial electrochemical studies of the V(IV)/V(V) and the V(II)/V(III) redox couples in 1985 [48, 49] and the first demonstration of an all-vanadium redox flow cell in 1986 [50] by Skyllas-Kazacos and co-workers, VRBs have been the focus of

intensive research, development, demonstration, and deployment activities for more than two decades. These efforts have culminated in several pilot plant scale or utility scale installations worldwide [31]. The electrode reactions of a VRB are:

Positive electrode:	$VO_2^+ + 2H^+ + e^- \rightleftharpoons VO^{2+} + H_2O$	$E^0 = +0.991\,V$
Negative electrode:	$V^{3+} + e^- \rightleftharpoons V^{2+}$	$E^0 = -0.255\,V$
Total reaction:	$VO_2^+ + V^{2+} + 2H^+ \rightleftharpoons VO^{2+} + V^{3+} + H_2O$	$E = 1.246\,V$

This system typically uses sulfuric acid as the electrolyte with a proton exchange membrane. While a porous separator could be used, for high efficiency operation, ion-selective membranes are generally preferred as vanadium crossover leads to losses in coulombic efficiency. At present, Nafion is the membrane of choice as V(V) is a powerful oxidizing agent, which can attack cheaper hydrocarbon-based ion selective membranes [21]. The redox reactions of different vanadium species have displayed reversibility and high activity on carbon based electrodes. Moreover, Li et al. discovered the catalytic effects of bismuth nanoparticles on V(II)/V(III) [51] and of niobium oxide nanorods on both V(II)/V(III) and V(IV)/V(V) [52], which have been shown to further enhance the energy efficiency of the VRB by more than 10 %.

One challenge of VRBs is the low energy density (<25 Wh/L), which is, at least partially, restricted by the low solubility of $VOSO_4$ (<1.7 M), which is sensitive to both acid concentration (3–4 M H_2SO_4) and solution temperature (10–40 °C) [53]. Recently, Li et al. developed sulfate-chloride mixed acid electrolyte that solubilizes V(V) in the form of $VO_2Cl(H_2O)_2$ up to 2.5 M, which corresponds to a 70 % improvement of the battery capacity compared to the conventional sulfate based electrolyte [54]. A 1 kW/1 kWh prototype VRB system using the mixed acid electrolyte has been demonstrated [55] and the underlying patents are being licensed by several companies. A second challenge for VRB technologies is the high cost of vanadium, reportedly 43 % of total cost for 1 MW/4 MWh mixed acid system [32]. This may set a floor for the potential system costs despite reductions enabled by mass production and engineering improvements. Alternative approaches are exploring the use of bromine polyhalide positive electrolytes, which leverages the higher solubility of vanadium in the presence of halides and the lower cost of bromine-based electrolytes [30, 31]. However, the aforementioned challenges with ICB and PSB systems; namely species crossover and bromine toxicity, are re-introduced.

3.1.2 Organic Redox Active Molecules

Recently, electroactive organics have been explored as active materials in aqueous RFBs and may open new avenues to meet the stringent grid storage cost targets. Indeed, organic molecules may offer several advantages over inorganic molecules. First, they are often comprised of earth-abundant elements (carbon, hydrogen, oxygen, nitrogen, sulfur, etc.), and thus, their cost and availability is less

constrained by the production and reserves of key elements (e.g., vanadium). Moreover, while transition metals must be mined and purified from ore, organic materials may be synthesized in sustainable fashion using green chemistry routes [56]. Second, while inorganic redox couples are restricted by the known periodic table, a broader array of organic redox-active molecules are available, allowing for the realization of new redox couples. Third, key electrochemical and physical properties (e.g., redox potential, solubility) can be tailored via modification of the redox moiety or the surrounding molecular structure. Further, a number of organics are known to undergo two electron transfer (e.g., quinones), which may lead to higher intrinsic capacities and thus, higher cell energy densities. These design degrees of freedom allow for a wide array of potential storage materials to be contemplated and for high throughput computational tools to be leveraged to drive the discovery and development process. However, as with any emerging materials, a number of unanswered questions exist including organic stability in acidic electrolytes and the organic solubility in aqueous media. Below, we highlight recent developments in organic aqueous RFBs.

Huskinson et al. studied the electrochemistry of 9,10-anthraquinone-2,7-disul phonic acid (AQDS) and demonstrated its applicability as the low potential compound in a AQDS-bromide aqueous redox flow cell [57]. AQDS undergoes a reversible, 2-electron transfer process on the glassy carbon electrode. Excitingly, the reported reaction kinetics were one to three orders of magnitude faster than many common redox couples Fe^{2+}/Fe^{3+}, Cr^{2+}/Cr^{3+}, VO^{2+}/VO_2^{+}, V^{2+}/V^{3+}, Br_2/Br^{-}, and S_4^{2-}/S_2^{2-} on similar carbon surfaces. The electrode reactions are:[2]

Positive electrode:	$Br_2 + 2e^- \rightleftharpoons 2Br^-$	$E^0 = +1.087\,V$
Negative electrode:	$AQDS + 2H^+ + 2e^- \rightleftharpoons AQDSH_2$	$E^0 = +0.213\,V$
Total reaction:	$Br_2 + AQDSH_2 \rightleftharpoons 2Br^- + AQDS + 2H^+$	$E = 0.874\,V$

Promising cycling performance and capacity retention was obtained using a benchtop cell (Fig. 3). Specifically, the cell was operated at a large current density (0.5 A/cm^2) with a high current efficiency ($\sim$99 %) and low capacity degradation (0.78 %/cycle). Since energy density is directly proportional to the number of electrons transferred by the redox active compound, the 2-electron transfer redox event of AQDS is highly favorable in the application of redox flow batteries. Moreover, via DFT-informed molecular design, the researchers were able to identify a more promising second generation AQDS derivative with one hydroxyl group on each benzene ring (1,8-dihydroxy-9,10-anthraquinone-2,7-disulphonic acid). Compared to AQDS, the derivative displayed a lower redox potential (consequently, a higher cell voltage) and higher kinetic rate constant, which not only produces a more favorable low potential compound, but also validates the applicability of computationally directed research for RFBs. Based on this work, the authors further explored the long-term cycling performance of the AQDS/Br_2 cell

[2]Determined by CV of 1 mM AQDS + 1 M H_2SO_4 on a glassy carbon electrode versus SHE.

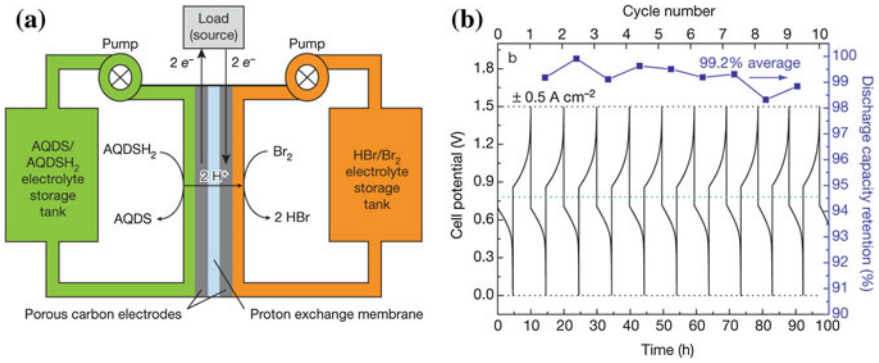

Fig. 3 **a** Cell schematic. Discharge mode is shown; the *arrows* are reversed for electrolytic/charge mode. $AQDSH_2$ refers to the reduced form of AQDS. **b** Constant-current cycling (0.5 A/cm^2) at 40 °C using a 3 M HBr + 0.5 M Br_2 solution on the positive side and a 1 M AQDS + 1 M H_2SO_4 solution on the negative side. Discharge capacity retention is indicated for each cycle [57]. Reproduced with permission. Copyright 2014 Nature

containing 0.1 L AQDS (1 M) and H_2SO_4 (1 M) on the negative side and 0.12 L Br_2 (0.5 M) and HBr (3 M) on the positive side with a Nafion 115 membrane separating the electrolytes [58]. The cell showed good stability at 100 % state-of-charge and 0.75 A/cm^2 over 750 cycles with an average discharge capacity retention and current efficiency as high as 99.84 and 98.35 %, respectively.

Beyond anthraquinone, the fundamental electrochemistry of other quinonoid compounds such as benzoquinone and naphthoquinone in aqueous systems have been thoroughly studied [59, 60], paving the way for their new applications in RFBs. Huskinson et al. reported the cyclic voltammetry results of 1,4-benzoquinone in neutral solution with high reversibility on both glassy carbon and platinum disc electrodes [61]. Moreover, they also studied the cycling performance of 0.1 M benzoquinone as the positive electrolyte couple with hydrogen reduction reaction with a theoretical cell voltage of ~0.70 V in acidic electrolyte using I-V polarization curve. The authors pointed out that the cell performance was primarily restricted by mass transport of benzoquinone due to its limited solubility whereas higher flow rate improved the peak power density and limiting current density. Xu et al. investigated the electrochemical behavior of 4,5-dihydroxybenzene-1,3-disulfonic acid disodium salt (Tiron) as a high potential compound in the application of aqueous redox flow batteries. Constant current electrolysis (vs. a lead counter electrode) was performed on Tiron (0.05 M) in a H_2SO_4 solution (3 M) [62]. The proposed reaction mechanism involves a reversible 2-electron transfer process followed by the addition of a hydroxyl group and a subsequent reversible 2-electron transfer process, which is also known as an ECE (electrochemical–chemical–electrochemical) process (Fig. 4). The reversible 2-electron transfer redox reaction between compound 3 and compound 4 at 0.96 V makes this redox couple an ideal high potential compound for aqueous redox flow batteries. Tiron, herein, serves as a starting material due to its commercial availability and low price.

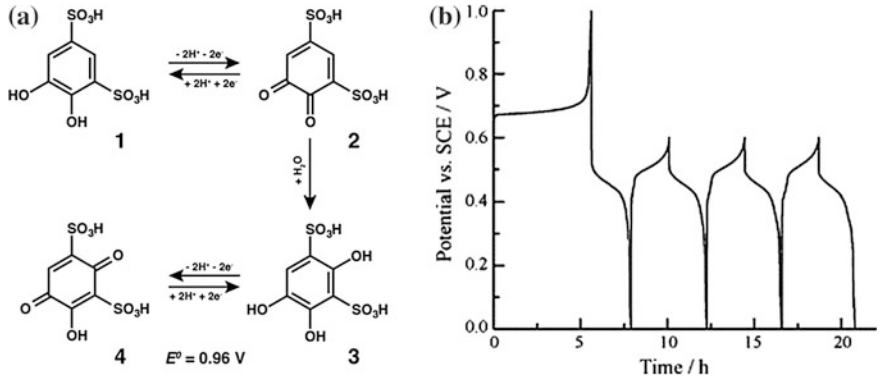

Fig. 4 **a** The mechanism of the redox reaction of 4,5-dihydroxybenzene-1,3-disulfonic acid. **b** Electrolytic characterization of tiron in 3 M H_2SO_4 at 298 K with a lead counter electrode [62]. Reproduced with permission. Copyright 2010 Electrochimica Acta

Combining Tiron and AQDS as the high potential and low potential redox active compounds, respectively, Yang et al. reported an all organic, aqueous redox flow cell with an open circuit voltage (OCV) of ~0.75 V [100 % state of charge (SOC)] [63]. A demonstration cell was operated using 0.2 M Tiron (positive side), 0.2 M AQDS (negative side), and 1 M H_2SO_4 (electrolyte) at a current density of 8 mA/cm^2 and a flow rate of 1000 mL/min, and displayed high current efficiency and acceptable capacity retention. In this paper, the authors also pointed out that the strong interaction between the ionized quinonoid species (R-SO_3^-) and water results in the low diffusion coefficient of the quinone based redox active molecules. Corroborating this statement, computational analysis of the I-V relationship revealed that lowering mass transfer resistance is critical to achieving a high operating current density in this type of redox flow cell.

3.2 Redox Active Compounds in Non-aqueous Flow Cells

As compared to their aqueous counterparts, non-aqueous RFBs are in their infancy. Transitioning from aqueous to non-aqueous electrolytes offers a wider window of electrochemical stability that enables cell operation at higher voltages. Indeed, depending on the salt, solvent, and electrode material, the stability window for non-aqueous electrolytes can span greater than 4 V [64]. Higher cell voltage leads to higher energy density, and typically to higher efficiency as well. These benefits promise to reduce cost of energy and to lessen system footprints that may enable specific applications such as energy storage in an urban environment. In addition, a broader selection of redox materials may be available due to either the wider potential window or the variety of available non-aqueous solvents. However, this promise must be balanced with the challenges associated with non-aqueous

electrolyte, including increased cost, reduced ionic conductivity, and other unfavorable physical properties (e.g., flammability). Understanding and balancing these competing factors will be key to determining the true value of non-aqueous RFBs. Below, we highlight recent research activities in the investigation of redox active compounds for non-aqueous flow cells.

3.2.1 Metal-Centered Coordination Complexes

As a natural extension of the studies conducted on transition metals for aqueous RFBs, metal-centered coordination complexes have been investigated for use in non-aqueous systems. The structure of a metal-centered coordination complex can be expressed as $[ML_n]^{z+}$ where M is a transition metal center (i.e., ruthenium, iron, vanadium, chromium, manganese, nickel, etc.). L is a ligand [i.e., acetylacetonate ($acac^-$), 2,2′-bipyridine (bpy), phenanthroline (phen), etc.], n is the number of ligands (typically n = 3 for bidentate ligands), and z is the total charge that combines the valence of the metal center and the charge of the ligand. Because an entire compound must be neutral, a counter ion is necessary if z is not zero. Using $[Ru(bpy)_3]$, $[Ru(acac)_3]$, and $[Ru(phen)_3]$ as examples, Fig. 5a–c depict the bonding environment of the ruthenium metal center as well as 2-D structures of 2,2′-bipyridine, acetylacetonate, and phenanthroline, respectively. While the metal center provides the electrochemical activity of $[ML_n]$, the coordinating ligands plays a pivotal role in determining a number of key parameters of the complex, such as the solubility, diffusivity, reversibility, and redox potential of each electron transfer event. Moreover, non-innocent (redox active) ligands may store additional charge thus increasing the intrinsic capacity of the complex [65]. A multi-step redox process with a sufficient potential difference enables the use of the same redox active compound as both the high potential and the low potential compound, which alleviates the concern of cross contamination. To date, most systems employ ACN and a non-coordinating salt [e.g., tetraethylammonium tetrafluoroborate ($TEABF_4$)] as the solvent and the supporting salt, respectively, with an anion exchange

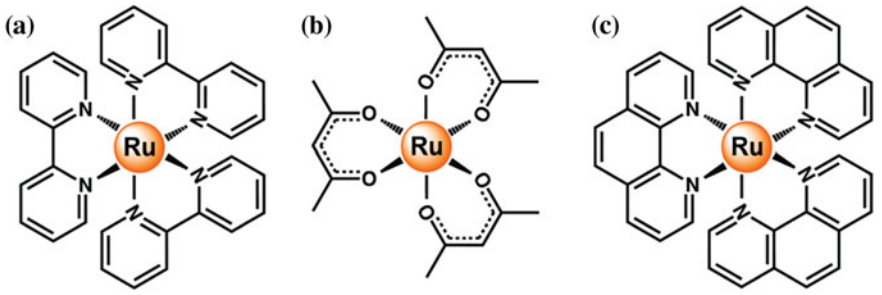

Fig. 5 The molecular structures of (A) $[Ru(bpy)_3]$, (B) $[Ru(acac)_3]$, and (C) $[Ru(phen)_3]$

Table 4 Non-aqueous redox flow batteries based on metal-centered coordination complex

Reactions	Electrolyte	Cell voltage (V)	Reference
$[Mn(IV)(acac)_3]^+ + e^- \rightleftharpoons Mn(III)(acac)_3$ $Mn(III)(acac)_3 + e^- \rightleftharpoons [Mn(II)(acac)_3]^-$	0.5 M $TEABF_4$ Acetonitrile	1.1	[66]
$[Ru(IV)(acac)_3]^+ + e^- \rightleftharpoons Ru(III)(acac)_3$ $Ru(III)(acac)_3 + e^- \rightleftharpoons [Ru(II)(acac)_3]^-$	0.05 M $TEABF_4$ Acetonitrile	1.77	[67]
$[Co(III)(acacen)]^+ + e^- \rightleftharpoons Co(II)(acacen)$ $Co(II)(acacen) + e^- \rightleftharpoons [Co(I)(acacen)]^-$	0.1 M $TEABF_4$ Acetonitrile	2.0	[68]
$[V(IV)(acac)_3]^+ + e^- \rightleftharpoons V(III)(acac)_3$ $V(III)(acac)_3 + e^- \rightleftharpoons [V(II)(acac)_3]^-$	0.1 M $TEABF_4$ Acetonitrile	2.2	[69]
$[Fe(III)(bpy)_3]^{3+} + e^- \rightleftharpoons [Fe(II)(bpy)_3]^{2+}$ $[Ni(II)(bpy)_3]^{2+} + 2e^- \rightleftharpoons Ni(0)(bpy)_3$	0.05 M $TEABF_4$ Propylene carbonate	2.3	[70]
$[Ru(III)(bpy)_3]^{3+} + e^- \rightleftharpoons [Ru(II)(bpy)_3]^{2+}$ $[Ru(II)(bpy)_3]^{2+} + e^- \rightleftharpoons [Ru(I)(bpy)_3]^+$	0.1 M $TEABF_4$ Acetonitrile	2.6	[71]

membrane (AEM) to separate the positive and negative electrolytes. Table 4 summarizes several reported metal-centered coordination complexes and the cell voltage of the proposed non-aqueous redox chemistry.

Ruthenium-Centered Coordination Complex

In 1988, Matsuda et al. demonstrated the first non-aqueous redox flow cell using $[Ru(bpy)_3]^{2+}/[Ru(bpy)_3]^{3+}$ and $[Ru(bpy)_3]^{+}/[Ru(bpy)_3]^{2+}$ as the high potential and low potential couples, respectively, with an OCV of 2.6 V [71]. A static H-cell polarization experiment identified the efficiency/performance limiting reaction as $[Ru(bpy)_3]^{+}/[Ru(bpy)_3]^{2+}$, which might be due to a side reaction and/or the low stability of $[Ru(bpy)_3]^{+}$. A flow cell cycling experiment demonstrated the charge-discharge capability of the cell with a 1.2 V discharge voltage, a 40 % coulombic efficiency and a 47 % utilization efficiency at 5 mA/cm^2. Although the performance metrics of this cell were far from practical, this seminal work initiated the application of metal-centered coordination complexes to non-aqueous redox flow cells and triggered ensuing research interest in this area. More recently, Chakrabarti et al. investigated ruthenium acetylacetonate ($Ru(acac)_3$) that displayed two 1-electron transfer processes with ~1.77 V separation according to the cyclic voltammetry [67]. The charge/discharge performance of $Ru(acac)_3$ was studied in the H-cell configuration containing 40 mL $Ru(acac)_3$ (0.1 M), $TEABF_4$ (1 M), and ACN in each compartment. At the charge and discharge rate of 1 and 0.5 mA, respectively, the first cycle gave an energy efficiency of 74 % and the second cycle gave an energy efficiency of 57 %. Based on this work, a redox flow cell using Ru $(acac)_3$ as the active materials with two 2.5-L storage tanks and 5 cm × 5 cm active area was demonstrated [72]. For 0.02 M $Ru(acac)_3$, the optimum power output was

determined to be 35 mW at the discharge current density of 2.1 mA/cm^2 and the voltage efficiency is 52.1 % (at 100 % SOC). Increasing the concentration of Ru(acac)$_3$ to 0.1 M increased the current density and power output by a factor of 5 (at the same velocity) due to the improved mass transfer of the active species.

Vanadium-Centered Coordination Complexes

Thompson et al. investigated a series of metal acetylacetonates [M(acac)$_3$] (where M = V [73], Cr [74], and Mn [66]) for their potential application in non-aqueous redox flow batteries. Amongst these beta-diketonate candidates, [V(acac)$_3$] has been systematically studied to optimize the cell performance with respect to the electrode surface, the impurity concentration, and the electrolyte. Specifically, the influence of the electrode surface (glassy carbon, platinum, and gold) on the electrochemistry of [V(III)(acac)$_3$]^0/[V(IV)(acac)$_3$]$^+$ (positive electrolyte) and [V(II)(acac)$_3$]$^-$/[V(III)(acac)$_3$]^0 (negative electrolyte) was examined [75]. The positive electrode reaction exhibits fast and reversible kinetics on all electrode surfaces. In contrast, the negative electrode reaction is surface-selective and the kinetic constant of [V(II)(acac)$_3$]$^-$/[V(III)(acac)$_3$]^0 on a gold electrode is about 6.5 times higher than that on a glassy carbon electrode. As the main source of impurities, oxygen and water deteriorate the performance of [V(acac)$_3$] based, non-aqueous redox flow cells [69]. Oxygen may degrade the electrolyte and block the reduction reaction on the negative electrode while water can not only impede the kinetics on the negative electrode but also hinder the positive electrode reaction by forming vanadyl acetylacetonate [VO(acac)$_2$]. In addition, a range of solvents (ACN, dimethylformamide, hexane, tetrahydrofuran, dimethylcarbonate) and salts [tetraethylammonium tetrafluoroborate, tetrabutylammonium tetrafluoroborate, tetrabutylammonium hexafluorophosphate,(1-butyl, 3-methyl)imidazolium bis(trifluoromethanesulfonyl) imide] were screened aiming at improving the conductivity of the electrolyte and the solubility of [V(acac)$_3$] [76]. According to their results, ACN and TEABF$_4$ is still the optimal combination for [V(acac)$_3$]. However, even under carefully controlled conditions, the charge/discharge performance of [V(acac)$_3$] (in a stirred H-cell) was still not desirable with coulombic and energy efficiencies of 70 and 35 %, respectively at 50 % SOC and a discharge current of 0.014 mA/cm^2.

Recently, vanadium-centered coordination complexes using the non-innocent redox active ligand—maleonitriledithiolate [(mnt)$^{2-}$] were investigated for their potential application in non-aqueous RFBs [65]. It has also been demonstrated that the reduction of [V(mnt)$_3$]$^{2-}$ adds one electron to the vanadium (IV) center and the oxidation of [V(mnt)$_3$]$^{2-}$ removes one electron from the (mnt)$^{2-}$ ligand. Therefore, non-innocent ligands may store additional electrochemical energy beyond what can be accessed from the metal center. In addition, improved complex stability can be expected when electron transfer takes place on the ligand rather than involving metal-ligand bonding. The redox potential of V(III)/V(IV) is tunable by the selection of cation in the supporting electrolyte, which might be attributed to the decreased relative electrostatic stabilization of [V(mnt)$_3$]$^{2-}$ and the increased steric

shielding of the cationic charge. The cycling performance using 0.02 M $TEA_2[V(mnt)_3]$ in 0.1 M tetrabutylammonium hexafluorophosphate ($TBAPF_6$)/ACN as both the positive and the negative electrolyte with a battery separator (Tonen) demonstrated the rechargeability of the non-aqueous redox flow cell with ~90 % coulombic efficiency and good capacity retention, although the energy efficiency is <45 %.

Fe, Co, Ni Based Coordination Complexes

Recently, promising results were reported by Mun et al. using $[Fe(bpy)_3]$ and $[Ni(bpy)_3]$ as the high potential and low potential compounds, respectively [70]. The 1-electron transfer $[Fe(II)(bpy)_3]^{2+}/[Fe(III)(bpy)_3]^{3+}$ takes place at +0.65 V versus Ag/Ag^+ and the 2-electron transfer $[Ni(bpy)_3]^0/[Ni(II)(bpy)_3]^{2+}$ takes place at −1.66 V versus Ag/Ag^+, which results in the nominal cell voltage of 2.31 V. The redox stability of both reactions in $TEABF_4$ (0.05 M)/PC was verified by a 100 cycle CV on a glassy carbon electrode. The advantageous electrochemical properties of the redox active compounds were further validated by the constant current (0.8 mA/cm^2) cycling in a flow cell containing 0.4 M $[Fe(bpy)_3](BF_4)_2$ and 0.2 M $[Ni(bpy)_3](BF_4)_2$ in $TEABF_4$ (0.5 M)/PC, and an AEM. The OCV of the cell was 2.2 V and the coulombic and energy efficiencies of the cell were maintained at 90.4 % and 81.8 %, respectively, throughout the cycling. The utilization efficiency (based on the first charging phase) was 92.8 % of the theoretical capacity. However, the capacity of the cell decayed over time, which might be due to the crossover of redox active species. An improved capacity retention was observed by replacing $[Ni(bpy)_3]$ with $[V(acac)_3]$ in a non-flowing cell [77]. Besides the non-aqueous chemistries discussed above, several other combinations such as $[Ni(phen)_3]$-$[Fe(phen)_3]$, $[Co(bpy)_3]$-$[Fe(bpy)_3]$, $[Co(phen)_3]$-$[Fe(phendione)_3]$[3] have been evaluated as well, and their performances were similar to that of the $[Fe(bpy)_3]$-$[Ni(bpy)_3]$ cell [77].

Ferrocene Derivatives

Ferrocene is a well-known redox model compound for its superior electrochemical reversibility and stability in non-aqueous electrolytes, and has been widely adopted as an internal standard for electrochemical measurements [78]. However, ferrocene's low solubility (e.g., <0.1 M in carbonate-based solvent) restricts its use in RFBs for grid energy storage. Recently, Wei et al. described a structural modification strategy to greatly enhance the solubility of ferrocene [79]. Figure 6a shows the structure of the ferrocene derivative (Fc1N112-TFSI). As evidenced experimentally and computationally by nuclear magnetic resonance (NMR) and DFT, respectively, the

[3]phendione stands for 1,10-phenanthroline-5,6-dione.

quaternary ammonium cation accentuates the interaction between the ionic pendant and the polarizable oxygen atoms on the carbonate solvent molecules. As a result, the as-prepared ionic-derivatized ferrocene compound can be dissolved in a carbonate based electrolyte [1.2 M LiTFSI in the mixture of ethylene carbonate (EC)/propylene carbonate (PC)/ethyl methyl carbonate (EMC) (4:1:5 by weight)] up to 0.85 M—more than 20 fold higher than the solubility of pristine ferrocene in the same electrolyte. Besides advancing the solvation chemistry, the quaternary ammonium cation also induces the electron withdrawing effect on the ferrocene moiety, which increases the redox potential of the ferrocene derivative by 0.23 V as compared to pristine ferrocene. Stable half-cell cycling performance of 0.1 M Fc1N112-TFSI with a lithium foil negative electrode is shown in Figs. 6b and c, further validating the electrochemistry of the compound. Furthermore, using a hybrid lithium-graphite negative electrode and appropriate additive (15 wt% fluoroethylene carbonate) in the electrolyte, the cycling performance of 0.8 M Fc1N112-TFSI was demonstrated at 1.5 mA/cm^2, resulting in 90 % coulombic efficiency, 76 % energy efficiency, 0.93 %/cycle degradation of discharge capacity.

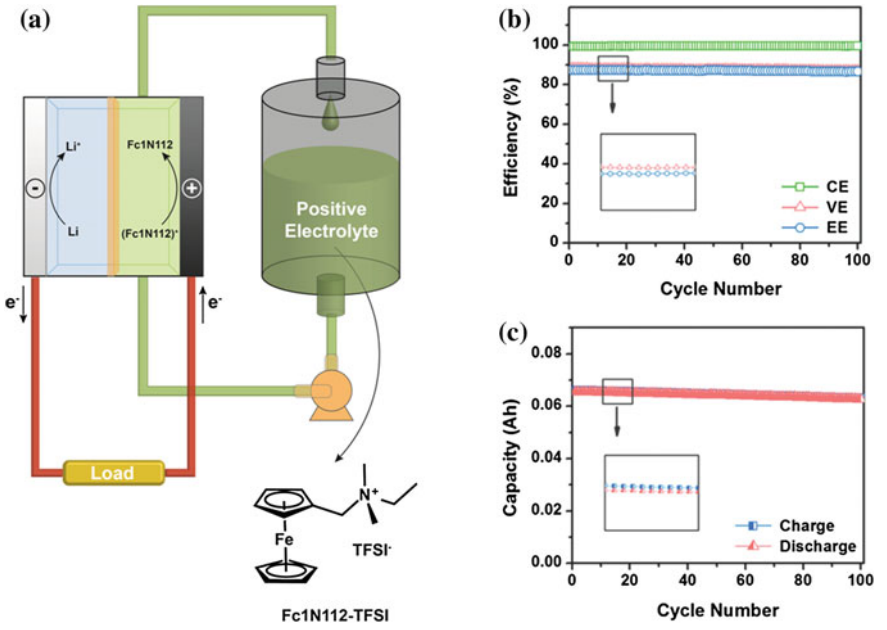

Fig. 6 **a** Cell schematic (discharge mode) and the molecular structure of Fc1N112-TFSI. **b** Coulombic (CE), voltage (VE), and energy (EE) efficiencies and **c** capacities of the half-cell test using 0.1 M Fc1N112-TFSI in 1.0 M LiTFSI in EC/PC/EMC with 5 wt% FEC at a current rate of 3.5 mA/cm^2 and a flow rate of 40 mL/min [79]. Reproduced with permission. Copyright 2014 Advanced Energy Materials

3.2.2 Organic Redox Active Molecules

Metal-centered coordination complexes are usually bulky, resulting in large molecular weights, and consequently, if not offset by multiple electron transfer events, small specific capacities (Mol. Cap. = nF/3.6*MW [Ah/kg]). In this regard, redox active organic molecules may offer the advantage of lower molecular weights and multi-electron transfer. Further, given the variety of non-aqueous solvents, redox active organic molecules may achieve higher solubilities, with fewer molecular modifications, than in aqueous electrolytes. For example, sulfonic groups (MW = 80 g/mol) are often attached to improve the organic solubility in aqueous electrolyte but these modifications can lower intrinsic capacity and may lead to less favorable properties (e.g., slower diffusion). In contrast, numerous functional groups are accessible for engineering the redox-active compounds in non-aqueous electrolytes, which enables rationally designed molecular modifications towards improved performances such as enabling multi-electron transfer, increasing solubility, improving the electrochemical reversibility, and shifting the redox potential.

Organic Molecules

Over the past decade, a wide variety of redox active organic materials have been investigated for use as solid electrodes in rechargeable Li-metal and Li-ion cells as well as for performance-enhancing solution-phase additives for advanced batteries [56, 80, 81]. For Li-metal and Li-ion cells, active material insolubility is desirable without tethering the discrete monomers to a polymeric backbone (lowering electrode capacity). In general, this can be pursued through enhanced polarity, π-π stacking, or reversible polymerizations. Despite these efforts, dissolution remains a key performance-limiting challenge for organic materials, especially at different charge states. A number of highly engineered redox active molecules have been developed as redox shuttles for overcharge protection in advanced batteries including phenothiazines, nitroxide-based radicals (vide infra), and substituted dimethoxybenzenes [82]. A number of these organic materials can be employed for non-aqueous RFB applications.

Brushett et al. reported the proof-of-concept study of an all-organic, lithium-ion based, non-aqueous redox flow cell using 2,5-di-tert-butyl-1,4-bis (2-methoxyethoxy)benzene (DBBB) and 2,3,6-trimethylquinoxaline (TMQ) in 0.2 M $LiBF_4$/PC with a theoretical OCV of 1.54 V (Fig. 7a) [83]. A wealth of knowledge from the development and optimization of electrolytes for Li-ion batteries [64, 84] can be leveraged to inform the design and construction of Li-ion based non-aqueous RFBs, which further enriches the selection of solvent and salts. As a product of molecular engineering, DBBB was originally designed for the overcharge protection of lithium-ion batteries [85], which requires a high redox potential, high electrochemical reversibility, moderate solubility, and high chemical compatibility. All of these properties are in perfect alignment with the criteria of redox active compounds in non-aqueous RFBs. Moreover, it has been determined

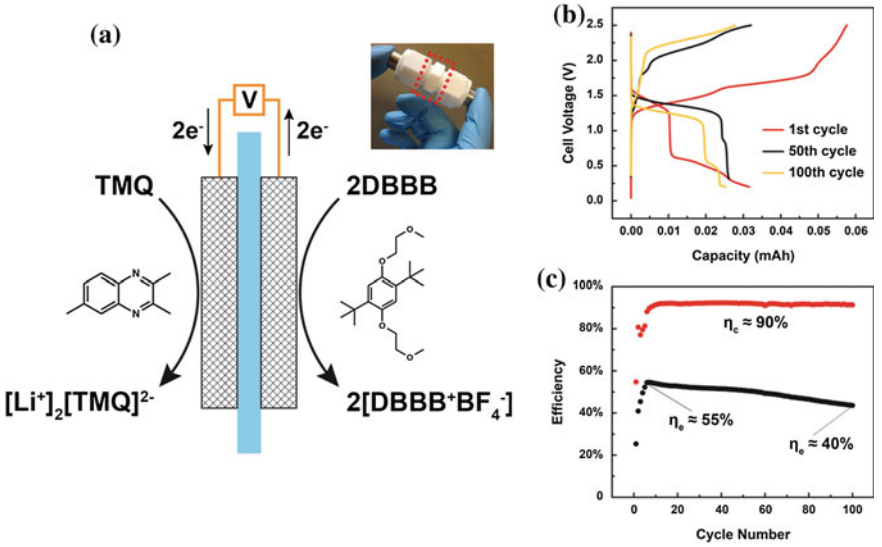

Fig. 7 **a** The image of Swagelok® cell and the corresponding reactions on the positive and negative electrodes during charging. **b** The 1st, 50th, and 100th constant current charge-discharge profiles. **c** The coulombic and energy efficiency over 100 cycles

that the rate constant and diffusivity of DBBB are comparable to those of ferrocene [86]. Quinoxaline, a commercially available compound with a molecular weight of only 130 g/mol, has displayed very high solubility (~7 M in most solvents) and promising electrochemical behavior in 0.2 M $LiBF_4$/PC. The addition of methyl groups on the conjugated rings not only enhances the reversibility of electron transfer, but also lowers the redox potential to a more negative value. The charge–discharge of the proposed system was demonstrated for 100 cycles in a non-flowing, Swagelok® cell configuration with lithiated Nafion 117 as the membrane, and displayed average coulombic and energy efficiencies of ~90 and ~50 %, respectively (Fig. 7b, c). Although the cell performance is far from being optimized, this archetypical work represents the baseline of organic redox active molecules for non-aqueous RFBs, and more importantly, provides a guideline for the future development of energy storage strategy in this category with higher energy density. To this end, more recent efforts have focused on the optimization of the positive electrolyte in terms of improving the conductivity and the solubility of DBBB in a range of carbonate based solvents and their mixtures [propylene carbonate (PC), ethylene carbonate (EC), dimethyl carbonate (DMC), diethyl carbonate (DEC)] with commonly used lithium salts (LiTFSI, $LiBF_4$, $LiPF_6$) in a high-throughput, automated screening platform [86]. The best combination of solubility and conductivity (at 25 °C) was obtained as 0.6 M (DBBB) and 5.25 mS/cm, respectively, in 0.6 M $LiPF_6$ in a ternary mixture of PC:EC:DMC (0.08:0.12:0.8). In addition, higher solubility of DBBB can be expected in ether

based solvent due to the presence of methoxymethyl group in the solute and solvent.

The superior electrochemistry of anthraquinone derivatives has not only found use in aqueous system as discussed in Sect. 3.1.2, but also attracts attention in non-aqueous RFBs. Wang et al. reported the structural modification of pristine anthraquinone by adding two triethylene glycol monomethyl ether groups onto the 1 and 5 carbons [87]. The adapted anthraquinone derivative showed a significantly improved solubility in non-aqueous polar solvent such as PC. This modification strategy towards the enhancement of solubility has recently been rationalized by DFT calculations [88]. Cyclic voltammetry of this compound displayed two 1-electron transfer processes centered at 2.82 and 2.50 V versus Li/Li^+ in 1 M $LiPF_6$/PC. The step-wise redox activity was also captured galvanostatically in a non-flowing, half-cell measurement. Moreover, this anthraquinone derivative based non-aqueous redox flow cell displayed high-energy efficiency ($\sim$82 %) and relative stable discharge energy density (with an average degradation rate of 0.08 mAh/L/cycle) in the cycling experiment at 0.1 mA/cm^2 for 40 cycles.

Using DFT calculations, Hernández-Burgos et al. investigated the effect of heteroatoms and substituents on the redox potential and stability of quinone based and other carbonyl based organic redox active molecules for energy storage applications [89]. As a rule, electron-withdrawing groups result in a positive shift of the redox potential while electron-donating groups result in a negative shift of the redox potential. Higher potential compounds tend to be less stable than the lower potential compounds, and the anionic species are predicted to be more stable than the neutral species. Furthermore, molecular engineering can also be realized by replacing the C atom with a heteroatom such as N, O, or S, especially for a five-membered ring, which will unburden the capacity penalty imposed by the increased molecular weight from the substituent. The same group also formulated a unique method to tune the redox potential of a carbonyl based organic redox active molecule by exploring the effect of cations in the supporting electrolyte as observed by RDV and verified by DFT [90]. Taking 1,2-di(thiophen-2-yl)ethane-1,2-dione (DTED) as an example, in the presence of a non-coordinating salt (tetrabutylammonium perchlorate), there are two 1-electron transfer processes observed at −1.36 and −2.20 V versus Ag/Ag^+. In the presence of a lithium salt ($LiClO_4$), the first reduction reaction slightly increases to −1.35 V and the second one noticeably increases to −1.80 V versus Ag/Ag^+, which can be explained by the stabilization effect of Li^+ on the anionic DTED due to its smaller size than that of $(TBA)^+$. In the presence of a magnesium salt [$Mg(ClO_4)_2$], the two 1-electron transfer processes merge to one 2-electron transfer process at dramatically higher potential (−1.11 V vs. Ag/Ag^+), which can be attributed to an even smaller ion with multiple charges. Therefore, this provides a flexible strategy for adjusting the redox potential of electroactive species based on the choice of supporting electrolyte ions according to their role as a high potential or low potential compound. While organic active materials in non-aqueous environments have the potential to enable high energy density storage, several key questions about the stability and solubility of active materials remain, particularly in their charged states. Furthermore, while a broad

array of materials are available, archetypical redox families and resulting cell chemistries with common ion exchange have yet to be developed and exploited. Establishing and testing these baseline systems is a critical next step.

Stable Radicals

Stable radicals are sub-valent compounds with an unpaired electron, which is stabilized via steric protection of the radical center and/or delocalization of the unpaired electron throughout the molecular structure. An important feature of stable organic radicals is the oxidation and reduction reactions producing closed-shell cations and anions via simple one-electron transfer outer-sphere reactions with no broken or formed chemical bonds. Often, but not always, these reactions are very fast and reversible. Certain classes of stable radicals, most notably nitroxides, are both durable and reactive under specific conditions, and thus are of interest as charge storage materials. Indeed, significant efforts by Nishide and co-workers have focused on developing organic radical batteries based on stable radical monomers tethered to polymeric backbones [91, 92]. Efforts by Buhermester et al. and Nakahara et al. have focused on understanding and exploiting nitroxide-based radicals, typically derivatives of 2,2,6,6-tetramethyl-1-piperidinyloxy (TEMPO), as active materials in non-aqueous electrolytes (e.g., for overcharge protection) [93, 94]. More recently, stable radicals have been explored for RFB applications. Li et al. proposed a non-aqueous redox flow cell utilizing TEMPO and, a redox-active organic molecule, N-methylphthalimide (NMP), as the high potential and low potential species, respectively, in $NaClO_4$ (1 M) in ACN [95]. The measured rate constants of TEMPO and NMP are on the order of 10^{-1} and 10^{-2} cm/s, respectively, both of which are higher than that of ferrocene ($\sim 10^{-3}$ cm/s); the diffusion coefficients of TEMPO and NMP are in the order of 10^{-5} cm^2/s (10-fold higher than ferrocene). A constant current cycling in a non-flowing cell kept a high coulombic efficiency of 90 % for 20 cycles with an average charging and discharging voltages of 1.65 and 1.36 V, respectively. More recently, Wei et al. demonstrated a hybrid non-aqueous RFB using TEMPO as the positive electrolyte and lithium metal as the negative electrode [96]. As TEMPO is quite soluble in carbonate-based solvents (e.g., >2.0 M actives in the presence of supporting salt), high energy flow cells were proposed and demonstrated (>100 Wh/L). Initial results are very promising and further chemistry development may lead to a standard positive electrolyte system for non-aqueous RFBs.

4 New Configuration of Redox Flow Batteries

From Fe^{2+}/Fe^{3+} in aqueous electrolytes to organic radicals in non-aqueous electrolytes, the development of novel redox active compounds over the past 30 years has greatly enriched the options for the electrochemistry in flow batteries. However,

the cell design and operating principles of redox flow cells have remained, for the most part, similar to the original configuration proposed by Thaller in 1974 [97]. New paradigms that incorporate unique flow patterns, electrode geometries, and electrolyte compositions are critical for the next generation flow batteries. This section highlights recent advances in these areas and describes emerging flow cell technologies.

4.1 Cell Architecture and Flow Channel Configuration

In general, the conventional electro-reactor architecture of a redox flow cell utilizes flow-through graphite felt electrodes coupled with graphite plate current collectors. Alternatively, redox flow cells can adopt design paradigms from more mature electrochemical technologies, such as proton exchange membrane fuel cells, where advances in cell engineering have led to high-performance reactor stacks. As shown in Fig. 8a, a graphite plate is in close contact with a thinner electrode such as carbon paper. Compared to the flow-through configuration, different flow patterns such as parallel, serpentine, and interdigitated flow, can be engraved on the graphite plate (Fig. 8b). The compression of the carbon electrode can be controlled by incompressible gaskets with varying thicknesses. The improved performance of this zero-gap cell architecture with a serpentine flow channel has been verified by Aaron et al. for VRB in terms of high peak power density (557 mW/cm^2, 1 M vanadium and 4 M H_2SO_4, 50 mL reservoirs) compared to other cell architectures under similar experimental conditions [98].

Recently, Darling and Perry systematically investigated the influence of a flow channel configuration on the cell parameters of the high-potential redox couple [V(IV)/V(V)] in VRBs [99]. Specifically, pressure drop, ohmic resistance, and the

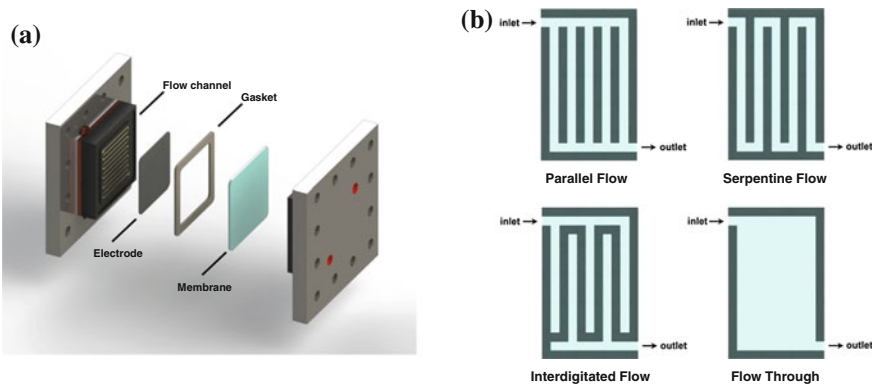

Fig. 8 **a** Exploded view of components in a redox flow cell with a flow channel. **b** Different flow channel configurations

limiting current were measured with respect to a combination of the electrode and channel configurations. The limiting current was measured at a constant voltage (0.4 V) and reflects the mass transfer limitation of the configuration. For the flow through configuration, the electrode was inserted in the flow channel whereas in the interdigitated and the parallel flow, electrodes were fixed on top of, but still in close contact, with the flow channel. The key results are that the interdigitated-flow carbon paper outperforms the conventional flow-through graphite felt in terms of pressure drop, which is directly related to pumping losses, and an increased cell resistance, which is directly related to ohmic loss, with equally efficient mass transfer. Therefore, the interdigitated flow configuration with carbon paper will be beneficial for high viscosity and low conductivity systems such as non-aqueous redox flow cells. While these experiments were conducted in a "half-cell" configuration, the results can lead to system level engineering and enable more combinatorial approaches towards enhancing flow battery performance.

4.2 Semi-solid Flow Batteries

In conventional redox flow cells, a flowing electrolyte carries redox active compounds to the surface of a static electrode that is in contact with a current collector to enable the electron transfer. Recently, Chiang and co-workers revolutionized this paradigmatic operating mode by introducing the concept of semi-solid flow batteries (Fig. 9a), which combines the features of high energy density lithium ion batteries and the advantage of scalability and flexibility from conventional redox flow cells [100]. The conventional static porous carbon electrode is replaced by a percolating network of nanoscale conductors that serve as the "dynamic electrode" in the semi-solid flow cell. In detail, electrochemically active compounds (redox, intercalation, etc.) and Ketjenblack carbon nanoparticles (<2 vol.%) are dispersed in the supporting electrolyte (salt + solvent) under sonication (Fig. 9b). This leads to the formation of a fractal nanoscale network within the electrolyte, which enables both electronic and ionic conduction. The aggregated carbon nanoparticles form a continuous flowable electrodes at a low volume fraction with the storage materials densely packed and in proximity to the carbon network. By pumping the suspension-based electrode through a channel, the carbon network contacts the current collector, enabling electron transfer into the suspension volume. The applicability of the proposed suspension has been demonstrated not only in static half-cells using lithium intercalation compounds such as $Li_4Ti_5O_{12}$ / $LiCoO_2$ but also in flow cells using $Li_3Ti_2(PO_4)_3$/$LiFePO_4$, in non-aqueous [100] and aqueous [101] systems, respectively. There are some key advantages associated with flowable electrodes:

- ***Solubility***—The energy density of a semi-solid flow battery is not limited by the solvation chemistry in the electrolyte, but rather depends on the rheology of the suspension (the suspension must still be flowable). For example, 20 vol.% $LiCoO_2$ (ρ = 5.06 g/cm^3, MW = 97.9 g/mol) can be easily dispersed in the

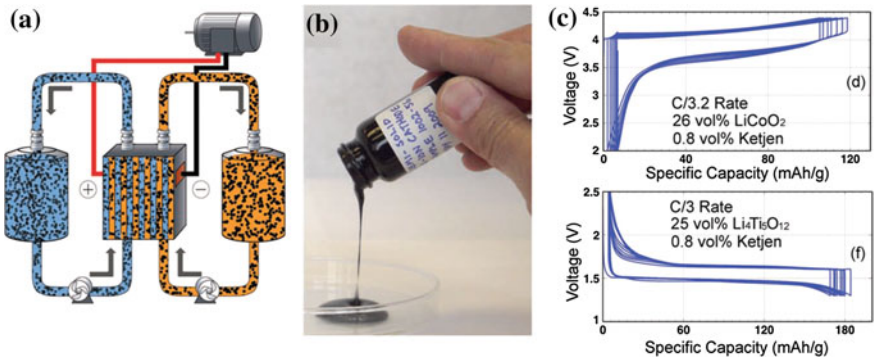

Fig. 9 **a** Scheme: semi-solid flow cell (SSFC) system using flowing lithium-ion cathode and anode suspensions could enable new models such as transportation 'fuels' tuned for power versus range, or cold versus warm climates, with flexible refueling and recycling options. **b** Fluid semi-solid suspension containing $LiCoO_2$ powder as the active material and Ketjenblack as the dispersed conductive phase, dispersed in alkyl carbonate electrolyte. **c** Galvanostatic charge/discharge curves for semi-solid suspensions having 26 vol.% $LiCoO_2$ (LCO) dispersed in 1.3 M $LiPF_6$ in an alkyl carbonate blend and 25 vol.% $Li_4Ti_5O_{12}$ (LTO) dispersed in 1 M LiPF6 in dimethyl carbonate [100]. Reproduced with permission. Copyright 2011 Advanced Energy Materials

suspension, corresponding to 10.2 M electrochemically active compound, which is much higher than any other maximum achievable solubility of redox active compounds in aqueous or non-aqueous systems [100].

- ***Surface area***—For the commonly used graphite felt (6 μm diameter fiber, 3 mm thickness), the specific surface area is ~0.33 m^2/g and the fraction of the fiber is ~6 vol.%. Therefore, the surface area of graphite felt in a cell is ~0.04 m^2/cm^3. For the carbon nanoparticles, the specific surface area is ~1400 m^2/g. Therefore, 1.5 vol.% Ketjenblack results in the surface area of the "nano-conductor" to be as large as ~42 m^2/cm^3 [102].
- ***Pumping efficiency***—Intuitively, the high viscosity suspension (~700 cP) would seem harder to pump than a solution (~50 cP for VRBs). However, if solution flow through a porous media is consider, as might be expected in an operating flow cell, the "wired-up" suspension becomes more attractive. For example, Fan et al. showed that for same flow channel length and diameter, the pressure drop of a suspension-based electrode through an open channel is actually three orders of magnitude lower than that of a solution-based electrolyte through a porous media (e.g., carbon electrode) with a 10 μm pore diameter [102].

Semi-solid flow cells with "wired" up electrolytes are an intriguing concept which can be applied to both soluble and insoluble chemistries [100, 101]. However, the unique properties that enable desirable electrolyte-level properties present new challenges for cell and system design. First, the electrolytes display non-Newtonian viscoelasticity properties (i.e., Herschel-Bulkley behavior), which confounds both

traditional cell design and pumping. Second, the electronic conductivity of the solution may lead to parasitic losses due to shunt currents throughout the system. Third, the impact of suspended particulates in the fluid may lead to increased pump and component wear (e.g., abrasion). Continued engineering improvements will be required to realize the full potential of this novel approach.

4.3 Hybrid Redox Flow Batteries

By definition, a hybrid redox flow cell involves plating and stripping of a redox active metal such as zinc, lithium, and lead, which generally serves as the negative electrode of a hybrid redox flow cell with the corresponding metal cation existing in the electrolyte. Given the high solubility in its discharged state (metal cations) and the zero mobility in its charged state (metal), the energy density limitation and the crossover concern of hybrid redox flow cells are not imposed by the low potential side. However, the concomitant penalty associated with the metal negative electrode is the formation of dendrites, which can puncture the membrane or separator, and consequently, short-circuit the battery.

4.3.1 Zinc-Based Redox Flow Batteries

A classic example of a hybrid redox flow battery is the zinc-halogen system, such as zinc-bromine, which can be traced back to 1885 [103], and was systematically re-evaluated as a secondary battery in 1964 [104]. Similarly, zinc–chlorine was investigated in the late 1970s and 1980s but was found to be environmentally hazardous (chlorine gas formation) and more complicated in a system level than the zinc-bromine chemistry. More recently, Lim et al. introduced a circulating aqueous electrolyte to the zinc-bromine battery (ZBB), which dramatically improved the performance of the system [105]. The electrode reactions of a ZBB are:

Positive electrode:	$Br_2 + e^- \rightleftharpoons 2Br^-$	$E^0 = +1.087\,V$
Negative electrode:	$Zn^{2+} + 2e^- \rightleftharpoons Zn$	$E^0 = -0.762\,V$
Total reaction:	$Br_2 + Zn \rightleftharpoons 2Br^- + Zn^{2+}$	$E = 1.849\,V$

The most attractive feature of ZBBs is the low cost of both zinc and bromine. In addition, the electrode polarization is very small due to the fast kinetics on both the positive and negative electrodes [105]. The circulation of electrolyte not only greatly improves the coulombic efficiency of the cell, but also alleviates the formation of dendrites on the negative electrode. However, self-discharge, resulting from the crossover of Br_2, is the primary concern of ZBBs, which can be aggravated by the formation of tribromide ions (Br_3^-) and other polybromide ions in the positive electrolyte. In practice, complexing agents such as quaternary ammonia salts are usually added to the positive electrolyte, which bind to these polybromide ions and

form a new, low-solubility liquid phase that is separated from the electrolyte [106]. In addition, a periodic stripping cycle, which aims to completely remove zinc from the negative electrode (100 % depth-of-discharge), is recommended to ensure a smooth zinc deposition during normal operation [14]. Commercially available ZBBs are designed for a 20-year service life with a modular 50 kWh unit and scalable to 500 kWh in a single enclosure and up to 4 enclosures (2 MWh) from a single point of system connection [107].

Besides the zinc-halogen systems, other zinc-based hybrid chemistries have been explored. One example is the alkaline zinc-ferricyanide redox flow cell that was demonstrated by Adams in 1979 [108]. The advantage of this zinc-ferricyanide redox flow cell includes high efficiency, high cell voltage, and low toxicity [109]. The electrode reactions are:

Positive electrode:	$[Fe(CN)_6]^{3-} + e^- \rightleftharpoons [Fe(CN)_6]^{4-}$	$E^0 = +0.358\,V$
Negative electrode:	$[Zn(OH)_4]^{2-} + 2e^- \rightleftharpoons Zn + 4OH^-$	$E^0 = -1.199\,V$
Total reaction:	$2[Fe(CN)_6]^{3-} + Zn + 4OH^- \rightleftharpoons 2[Fe(CN)_6]^{4-} + [Zn(OH)_4]^{2-}$	$E = 1.557\,V$

The system utilizes zinc and carbon as the negative and positive electrodes, respectively. On discharge, zinc is converted to a zincate ion ($[Zn(OH)_4]^{2-}$) which is then converted and stored in the negative electrolyte tank as ZnO. Similarly, sodium ferro- and ferricyanides are stored as precipitates in the positive electrolyte tank. This unique design of solid storage in the electrolyte tanks results in a smaller footprint, but in a more complex system management and temperature control.

Another example is the zinc-cerium redox flow cell developed by Clarke et al. in 2004 [110]. The electrode reactions are:

Positive electrode:	$Ce^{4+} + e^- \rightleftharpoons Ce^{3+}$	$E^0 = +1.720\,V$
Negative electrode:	$Zn^{2+} + 2e^- \rightleftharpoons Zn$	$E^0 = -0.7618\,V$
Total reaction:	$2Ce^{4+} + Zn \rightleftharpoons 2Ce^{3+} + Zn^{2+}$	$E = 2.482\,V$

Methanesulfonic acid is preferentially used as the electrolyte on both sides to increase the solubility of the metal cations [111]. Zinc-cerium chemistries enable a very high cell voltage. However, the concomitant parasitic reactions such as HER and OER must be avoided or minimized to achieve acceptable cell efficiencies.

4.3.2 Soluble Lead-Acid Flow Batteries

An extension of hybrid redox flow batteries is the "double hybrid" soluble lead-acid flow batteries (SLFBs) where deposition and dissolution of redox active compounds are involved in both high potential and low potential electrode reactions. Pletcher et al. explored the concept of SLFBs in 2004 [112], and have reported their systematic study in a series of papers [113–120]. The electrode reactions of a SLFB are:

Positive electrode:	$PbO_2 + 4H^+ + 2e^- \rightleftharpoons Pb^{2+} + 2H_2O$	$E^0 = +1.455\,V$
Negative electrode:	$Pb^{2+} + 2e^- \rightleftharpoons Pb$	$E^0 = -0.126\,V$
Total reaction:	$PbO_2 + Pb + 4H^+ \rightleftharpoons 2Pb^{2+} + 2H_2O$	$E = 1.581\,V$

As shown in Fig. 10, the electrolyte consists of lead (II) methansulfonate (up to 2 M) in a biodegradable methanesulfonic acid (1.5 M). Charging the cell results in metallic lead (Pb^0) being deposited at the negative electrode and lead (IV) dioxide at the positive electrode; discharging the cell results in Pb^{2+} being re-dissolved into the electrolyte from both electrodes. SLFBs differ from traditional lead-acid batteries in that, rather than residing on the electrodes in the form of $PbSO_4$, the lead methansulfonate is dissolved in methanesulfonic acid, which enables the flow functionality of SLFBs. Furthermore, the single redox active molecule (Pb^{2+}) existing in the electrolyte contributes two very attractive features of SLFBs compared to other redox flow batteries. (1) There is no need for an ion-selective membrane in the cell, and consequentially, (2) only one electrolyte storage tank is required. These key features allow for a simplified cell design and decreased footprint of the system, and in turn, greatly reduces the construction and maintenance cost of a SLFB.

However, similar to other hybrid redox flow systems where liquid-solid reactions occur, SLFBs suffer from Pb^0 dendrite formation on the negative electrode

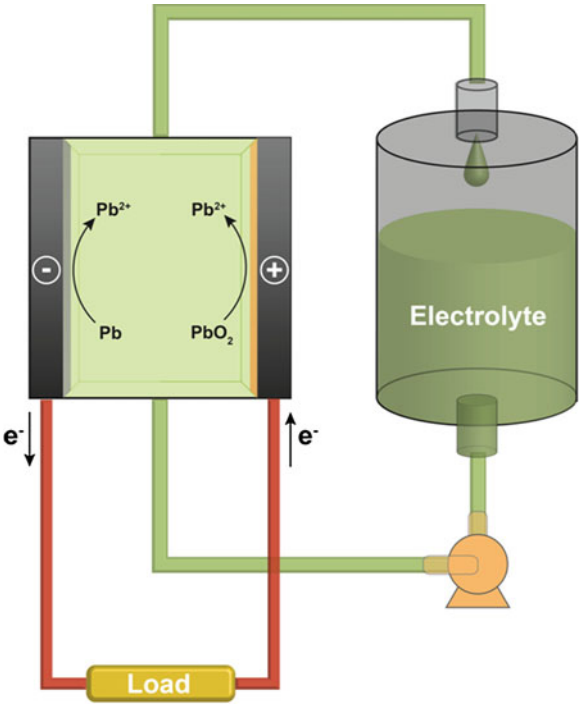

Fig. 10 Schematic of a soluble lead-acid redox flow battery

and more severely, irreversible PbO_2 polymorph (both α- and β-PbO_2) formation on the positive electrode, which dictates the low current density applied in SLFBs (typically <20 mA/cm^2). Recently, Verde et al. demonstrated that increased mass transfer results in the formation nanoscale PbO_2 and Pb^0 on the positive and negative electrodes, respectively, which effectively mitigates the polymorph and dendrite issues during charging [121]. In a beaker-cell configuration with sufficient stirring, their soluble lead-acid flow cell achieved an energy efficiency of ~79 % for 2000 cycles at 20 mA/cm^2. Continued efforts are needed in the development of novel flow reactor architectures that allow for faster mass transport of Pb ions across the electrode surfaces to minimize depletion layer thickness while keeping the pumping cost low.

4.3.3 Lithium-Aqueous Flow Batteries

Lithium metal is an extremely attractive negative electrode material due to its high theoretical specific capacity (3861.9 mAh/g), low electrochemical potential (−3.04 V vs. SHE), and possibility of coupling with a charged or discharged positive electrode material [122, 123]. However, despite significant efforts over the past 40 years, continued challenges with safety and efficiency during prolonged and/or high rate battery operation prevent the deployment of advanced Li batteries. However, emerging needs for high energy batteries for transportation applications (e.g., Li–metal oxide, Li–S, Li–O_2) continued to drive research and development. Indeed, over the past five years, progress has been made in enhancing cyclability and safety through the mechanically robust and chemically-stable solid-electrolyte membranes, based on ceramics, polymers or hybrid materials [124]. These advances may also be leveraged to develop hybrid flow systems where the lithium metal negative electrode is paired with a flowing positive electrolyte.

Lu and Goodenough demonstrated a hybrid redox flow cell using a lithium negative electrode in static non-aqueous electrolyte and a carbon positive electrode in circulating aqueous electrolyte with 0.1 M $K_3Fe(CN)_6$ as the redox active molecule [126]. The key design component is a sub-millimeter thick water stable lithium-ion conducting ceramic, $Li_{1+x+y}Al_xTi_{2-x}Si_yP_{3-y}O_{12}$, which enables Li-ion transfer between the two compartments. To avoid chemical reduction of the solid electrolyte on the lithium metal, two pieces of electrolyte soaked polypropylene separator (Celgard) were used. This concept can be extended to a wide range of aqueous redox couples (Fig. 11) many of which have been explored by different groups [127]. Recently, Zhao and Byon described a hybrid lithium-iodine redox flow cell and systematically investigated the influence of the concentration of redox active molecule, flow rate, discharge current, and temperature on the cell performance [128]. Figure 12a illustrates the configuration of the system. Lithium ion conductive Li_2O-Al_2O_3-TiO_2-P_2O_5 (LATP) solid electrolyte was employed to separate the positive and negative flowing electrolyte, and a layer of glass fiber was employed to separate the solid electrolyte and lithium metal. The electrode reactions are:

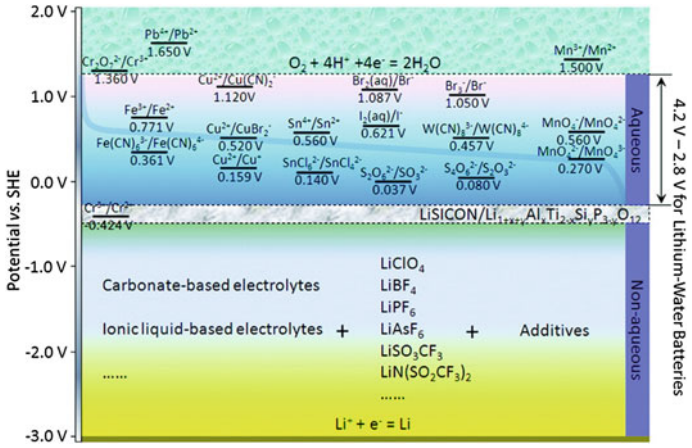

Fig. 11 Systems for lithium-aqueous batteries [125]. Reproduced with permission. Copyright 2011 Journal of the American Chemical Society

Positive electrode:	$I_3^- + 2e^- \rightleftharpoons 3I^-$	$E^0 = +0.536\,V$
Negative electrode:	$Li^+ + e^- \rightleftharpoons Li$	$E^0 = -3.040\,V$
Total reaction:	$I_3^- + 2Li \rightleftharpoons 3I^- + 2Li^+$	$E = 3.576\,V$

Lithium iodide is highly soluble in water, up to 12.4 M (25 °C), which can match the high capacity of the lithium negative electrode. The cycling data of the hybrid lithium-iodine battery are shown in Fig. 12b, where high coulombic efficiency (>99 %) and good capacity retention (>99 %) were obtained for 20 cycles. A key challenge for lithium-aqueous systems is the low ionic conductivity of the solid electrolyte, which is two orders of magnitude lower than that of non-aqueous electrolytes and three orders of magnitude lower than that of aqueous electrolytes. Therefore, greatly improved energy efficiency and higher charge/discharge rates for aqueous-non-aqueous based hybrid redox flow cells can be expected from more conductive solid electrolytes.

4.3.4 Lithium–Polysulfide Flow Batteries

In the pursuit of highly efficient, low cost energy storage systems, the lithium-sulfur (Li–S) hybrid battery is one of the most promising technologies due to its high theoretical energy density [129]. In a Li–S cell, lithium metal is applied as the negative electrode and solid-state sulfur as the positive electrode. The electrode reactions of a Li–S cell are:

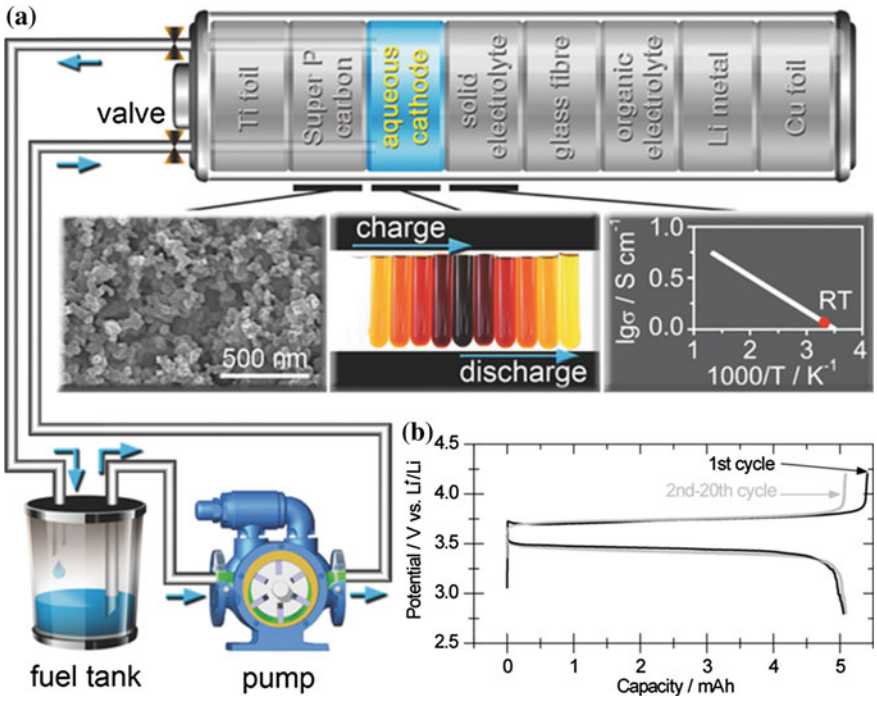

Fig. 12 **a** Schematic illustration of a cathode-flow mode aqueous Li–I battery equipped with an aqueous electrolyte reservoir and pump. The *center insets* from left to right are SEM image of the Super P carbon current collector, an image of color gradients of LiI aqueous electrolytes, and a graph of temperature-dependent ionic conductivity in lithium-ion-conducting LATP solid electrolyte (on the order of 10^{-4} S cm^{-1} at RT). The LiI electrolyte color in the *center-middle inset* corresponds to the depth of charge and discharge (0, 5, 15, 25, 50 and 100 % of charge and 0, 50, 75, 85, 95 and 100 % of discharge from left to right). **b** 20-times cycled charge/discharge profiles of CF/LiIB equipped with an aqueous electrolyte reservoir containing total 0.5 mL of 0.5 m of LiI aqueous electrolyte at a current rate of 2.5 mA/cm^2 and a flow rate of 150 μL/min [128]. Reproduced with permission. Copyright 2014 Advanced Energy Materials

Positive electrode:	$S + 2e^- \rightleftharpoons S^{2-}$	$E^0 = -0.476\,V$
Negative electrode:	$Li^+ + e^- \rightleftharpoons Li$	$E^0 = -3.040\,V$
Total reaction:	$2Li + S \rightleftharpoons Li_2S$	$E = 2.564\,V$

The theoretical capacity of sulfur ($S^0 \rightleftharpoons S^{2-}$) is 1672.0 mAh/g, which is 12.2, 19.7, and 22.6 times higher than that of $LiCoO_2$, $LiFePO_4$, and $LiMn_2O_4$ (assuming 0.5 Li^+ transfer per molecule), respectively. Ether-based electrolytes such as tetrahydrofuran (THF), 1,3-dioxolane (DOL), 1,2-dimethoxyethane (DME), tetraethylene glycol dimethyl ether (TEGDME) are commonly used in Li–S batteries. The evolution of S to Li_2S involves the formation of Li_2S_x intermediates that have varying solubilities in ether-based electrolytes. For example, when $8 \geq x \geq 6$, Li_2S_x

is highly soluble, while when x = 4, Li_2S_x is moderately soluble, and when x < 4, Li_2S_x is insoluble [130]. Since both positive and negative electrodes of conventional Li–S batteries are in the solid state, the soluble intermediates impose the most noticeable technical challenge in a Li–S cell, resulting in low coulombic efficiency (shuttle mechanism) and poor capacity retention (self-discharge) [131]. In addition, both S and Li_2S are electrical insulators, which limit the rechargeability and charge/discharge rate of Li–S batteries [129].

Lithium–polysulfide (Li–PS) flow batteries originated from Li–S batteries. Still using lithium metal as the negative electrode, Li–PS flow cells utilize a porous carbon electrode and soluble lithium polysulfides (Li_2S_x where $8 \geq x \geq 4$) as the positive electrode and positive electrolyte, respectively. The positive electrode reactions can be described as:

$$Li_2S_8(\text{soluble}) \rightleftharpoons Li_2S_6(\text{soluble}) \rightleftharpoons Li_2S_4(\text{soluble})$$

A full charge/discharge cycle between Li_2S_8 and Li_2S_4 corresponds to the theoretical capacity of 209.0 mAh/g S, which is still higher than that of the positive electrode materials in conventional lithium ion batteries. The cycle between Li_2S_8 and Li_2S_4 is realized by controlling cutoff voltages. The application of dissolved Li_2S_x species as the starting positive electrolyte in a Li–S cell was first demonstrated by Rauh et al. in 1979 [132], and the idea of a Li–PS flow battery was proposed by Manthiram et al. in 2013 [133]. It has been recently recognized that $LiNO_3$ can form a stable passivation layer on the surface of the lithium negative electrode, which effectively prevents the reaction between the dissolved Li_2S_x and lithium metal [134, 135]. Therefore, with $LiNO_3$ additive in the electrolyte, ion-selective membranes are not needed in a Li-PS flow cell. Based on this strategy, Yang et al. recently demonstrated the chemistry of Li–PS in a coin-cell configuration. In a constant capacity cycling experiment using 5 M Li_2S_8, the static Li-PS cell displayed superior cyclability at ~200 mAh/g S for more than 1500 cycles [136]. Recently, Fan et al. demonstrated the applicability of semi-solid carbon suspension as the high-surface area (42 m^2/cm^3) current collectors in a Li–PS flow cell [102]. In this proof-of-concept device, potentiostatic cycling experiment where the cell was charged at 2.5 V and discharged at 2.1 V to maintain all polysulfide species solubilized in the solution, the discharge capacity of the cell is 181 mAh/g S with a coulombic efficiency close to 100 %. Moreover, the percolating conductor network with extremely large surface area enabled deep cycling of polysulfide into the precipitation regime of Li_2S [102], which might be due to the mitigated insulating effect of Li_2S on the lower surface area carbon current collector. Therefore, much higher discharge capacity (393 mAh/g S) was achieved by extending the discharge voltage to 1.6 V so that the precipitation regime of Li_2S can be utilized. The coulombic efficiency remained above 99.5 % at the discharge rate of C/22 over 10 cycles.

5 Conclusions and Outlook

Stationary energy storage systems, in particular electrochemical energy storage systems, will play a pivotal role in the widespread integration of renewable, non-dispatchable energy sources (e.g., solar photovoltaic (PV), wind) and in the improvement of energy efficiency of the electric power sector. Redox flow batteries are particularly attractive for these applications due to their favorable combination of performance, cost, and safety. However, present generation technologies are not cost-competitive, which drives research and development efforts towards new redox chemistries, electrolyte formulations, and cell designs. Recent analysis by Darling et al. has indicated that both aqueous and non-aqueous RFBs have pathways to meeting long-term objectives for cost-effective energy storage [137]. As mentioned before, reductions in battery costs ($/kWh) can be achieved via lowering materials cost ($/kg) and increasing materials energy density (kWh/kg). Electroactive organic molecules, both as solo active materials or as components of metal-centered complexes, may offer a pathway forward through both metrics. In principle, organic materials can be synthesized via cost-effective routes and are less dependent on the production and reserves of key elements (e.g., vanadium in VRB). Moreover, the electrochemical and physical properties of electroactive materials can be tailored via modification of the redox moieties and the surrounding molecular structure. This may lead to the development of high capacity and highly soluble redox materials required for energy dense cell operation. To realize this promise, further efforts are needed in the identification and optimization of novel redox active materials, likely leveraging high throughput computations, and in validation of these materials within redox flow cells at high currents and extended cycling. Reductions in battery costs may also be achieved through advances in cell design and engineering. High performance electroreactors, often inspired by more mature electrochemical technologies (e.g., fuel cells), can reduce reactor size requirements and associated costs. Further, new reactor designs are required to efficiently employ non-aqueous chemistries with low ionic conductivity and high voltage, and mixed conductor suspensions that offer higher cell energy densities but frustrate traditional configurations. Together with an evolving regulatory environment, these R&D activities are expected to lead to the commercial success of RFB technologies in the near future and to the deployment of a range of new flowable storage concepts.

Acknowledgments The authors gratefully acknowledge financial support from the Joint Center for Energy Storage Research, an Energy Innovation Hub funded by the U.S. Department of Energy, Office of Science, Basic Energy Sciences, and from the Massachusetts Institute of Technology Energy Initiative's (MITei) Seed Fund Program. In addition, we thank Jarrod Milshtein and Apurba Sakti for stimulating discussions and for assistance in figure development.

References

1. International Energy Agency (2014) Key world energy statistics
2. Hojjati B, Wade SH (2012) US household energy consumption and intensity trends: a decomposition approach. Energy Policy 48:304–314
3. U.S. Energy Information Administration (2011) Annual energy review. http://www.eia.gov/totalenergy/data/annual/index.cfm/
4. Rising above the gathering storm: energizing and employing America for a brighter economic future. In: Committee on prospering in the global economy of the 21st century: an agenda for American science and technology; Committee on Science, Engineering, and Public Policy. National Academies Press, Washington, D.C., 2007
5. Ehleringer JR, Cerling TE, Dearing MD (2005) In: Ehleringer JR, Cerling TE, Dearing MD (eds) A history of atmospheric CO_2 and its effects on plants, animals, and ecosystems. Springer, New York
6. Stocker T, Qin D, Plattner G-K (2013) Climate change 2013: the physical science basis. Working group I contributions to the IPCC fifth assessment report of the intergovernmental panel on climate change
7. International Energy Agency (2012) Energy technology perspectives 2012: pathways to a clean energy system
8. Chu S, Majumdar A (2012) Opportunities and challenges for a sustainable energy future. Nature 488:294–303. doi:10.1038/nature11475
9. U.S. Department of Energy (2010) Smart grid system report
10. U.S. Department of Energy (2013) Grid energy storage
11. Akhil AA, Boyes JD, Butler PC, Doughty DH (2010) Batteries for electrical energy storage applications. In: Reddy T (ed) Linden's handbook of battery, Chap. 30, 4th edn. McGraw-Hill, New York
12. U.S. Department of Energy (2007) Basic research needs for electrical energy storage
13. International Energy Agency (2014) Technology roadmap: energy storage. http://www.iea.org/publications/freepublications/publication/name,36573,en.html. Accessed 10 April 2014
14. Electric Power Research Institute (2003) DOE handbook of energy storage for transmission and distribution applications
15. Akhil AA, Huff G, Currier AB, Kaun BC, Rastler DM, Chen SB, Cotter AL, Bradshaw DT, Gauntlett WD (2013) DOE/EPRI 2013 electricity storage handbook in collaboration with NRECA. Sandia National Laboratories
16. Electric Power Research Institute (2010) Electricity energy storage technology options
17. International Energy Agency (2013) Pumped storage provides grid reliability even with net generation loss. http://www.eia.gov/todayinenergy/detail.cfm?id=11991. Accessed 10 Oct 2014
18. ARPA-E. U.S. Department of Energy. Grid-scale rampable intermittent dispatchable storage. http://www.arpa-e.energy.gov/?q=arpa-e-programs/grids. Accessed 05 Jan 2015
19. U.S. Department of Energy (2014) Joint center for energy storage. http://www.jcesr.org. Accessed 05 Jan 2015
20. Shin S-H, Yun S-H, Moon S-H (2013) A review of current developments in non-aqueous redox flow batteries: characterization of their membranes for design perspective. RSC Adv 3:9095–9116. doi:10.1039/C3RA00115F
21. Schwenzer B, Zhang J, Kim S, Li L, Liu J, Yang Z (2011) Membrane development for vanadium redox flow batteries. ChemSusChem 4:1388–1406. doi:10.1002/cssc.201100068
22. Li X, Zhang H, Mai Z, Zhang H, Vankelecom I (2011) Ion exchange membranes for vanadium redox flow battery (VRB) applications. Energy Environ Sci 4:1147. doi:10.1039/c0ee00770f
23. Chakrabarti MH, Brandon NP, Hajimolana SA, Tariq F, Yufit V, Hashim MA, Hussain MA, Low CTJ, Aravind PV (2014) Application of carbon materials in redox flow batteries. J Power Sources 253:150–166. doi:10.1016/j.jpowsour.2013.12.038

24. Parasuraman A, Lim TM, Menictas C, Skyllas-Kazacos M (2013) Review of material research and development for vanadium redox flow battery applications. Electrochim Acta 101:27–40. doi:10.1016/j.electacta.2012.09.067
25. Li X, Sabir I (2005) Review of bipolar plates in PEM fuel cells: flow-field designs. Int J Hydrogen Energy 30:359–371. doi:10.1016/j.ijhydene.2004.09.019
26. Alotto P, Guarnieri M, Moro F (2014) Redox flow batteries for the storage of renewable energy: a review. Renew Sustain Energy Rev 29:325–335. doi:10.1016/j.rser.2013.08.001
27. Wang W, Luo Q, Li B, Wei X, Li L, Yang Z (2013) Recent progress in redox flow battery research and development. Adv Funct Mater 23:970–986. doi:10.1002/adfm.201200694
28. Leung P, Li X, de León CP, Berlouis L, Low CTJ, Walsh FC (2012) Progress in redox flow batteries, remaining challenges and their applications in energy storage. RSC Adv 2:10125–10156. doi:10.1039/C2RA21342G
29. Yang Z, Zhang J, Kintner-Meyer MCW, Lu X, Choi D, Lemmon JP, Liu J (2011) Electrochemical energy storage for green grid. Chem Rev 111:3577–3613. doi:10.1021/cr100290v
30. Weber AZ, Mench MM, Meyers JP, Ross PN, Gostick JT, Liu Q (2011) Redox flow batteries: a review. J Appl Electrochem 41:1137–1164. doi:10.1007/s10800-011-0348-2
31. Skyllas-Kazacos M, Chakrabarti MH, Hajimolana SA, Mjalli FS, Saleem M (2011) Progress in flow battery research and development. J Electrochem Soc 158:R55–R79. doi:10.1149/1.3599565
32. Viswanathan V, Crawford A, Stephenson D, Kim S, Wang W, Li B, Coffey G, Thomsen E, Graff G, Balducci P, Kintner-Meyer M, Sprenkle V (2014) Cost and performance model for redox flow batteries. J Power Sources 247:1040–1051. doi:10.1016/j.jpowsour.2012.12.023
33. LaMonica M (2013) Enervault novel battery technology. MIT Technol Rev. http://www.technologyreview.com/view/512736/startup-enervault-rethinks-flow-battery-chemistry/. Accessed 10 Sep 2014
34. Vanysek P (2014) Electrochemical series. In: Haynes WM (ed) CRC handbook of chemistry and physics, 95th edn. Taylor & Francis Group, Boca Raton, pp 5-80–5-89
35. Reid MA, Gahn RF (1977) Factors affecting the open-circuit voltage and electrode kinetics of some iron/titanium redox flow cells. NASA-TM X-73669
36. Wang W, Kim S, Chen B, Nie Z, Zhang J, Xia G-G, Li L, Yang Z (2011) A new redox flow battery using Fe/V redox couples in chloride supporting electrolyte. Energy Environ Sci 4:4068–4073. doi:10.1039/C0EE00765J
37. Lopez-Atalaya M, Codina G, Perez JR, Vazquez JL, Aldaz A (1992) Optimization studies on a Fe/Cr redox flow battery. J Power Sources 39:147–154. doi:10.1016/0378-7753(92)80133-V
38. Skyllas-Kazacos M, Grossmith F (1987) Efficient vanadium redox flow cell. J Electrochem Soc 134:2950–2953. doi:10.1149/1.2100321
39. Zhou H, Zhang H, Zhao P, Yi B (2006) A comparative study of carbon felt and activated carbon based electrodes for sodium polysulfide/bromine redox flow battery. Electrochim Acta 51:6304–6312. doi:10.1016/j.electacta.2006.03.106
40. Skyllas-Kazacos M (2003) Novel vanadium chloride/polyhalide redox flow battery. J Power Sources 124:299–302. doi:10.1016/S0378-7753(03)00621-9
41. Xue F-Q, Wang Y-L, Wang W-H, Wang X-D (2008) Investigation on the electrode process of the Mn(II)/Mn(III) couple in redox flow battery. Electrochim Acta 53:6636–6642. doi:10.1016/j.electacta.2008.04.040
42. Fang B, Iwasa S, Wei Y, Arai T, Kumagai M (2002) A study of the Ce(III)/Ce(IV) redox couple for redox flow battery application. Electrochim Acta 47:3971–3976. doi:10.1016/S0013-4686(02)00370-5
43. Bartolozzi M (1989) Development of redox flow batteries. A historical bibliography. J Power Sources 27:219–234. doi:10.1016/0378-7753(89)80037-0
44. Hagedorn N (1984) NASA redox storage system development project. NASA-TM-83677
45. Zhao P, Zhang H, Zhou H, Yi B (2005) Nickel foam and carbon felt applications for sodium polysulfide/bromine redox flow battery electrodes. Electrochim Acta 51:1091–1098. doi:10.1016/j.electacta.2005.06.008

46. Scamman DP, Reade GW, Roberts EPL (2009) Numerical modelling of a bromide–polysulphide redox flow battery: Part 1: modelling approach and validation for a pilot-scale system. J Power Sources 189:1220–1230. doi:10.1016/j.jpowsour.2009.01.071
47. Scamman DP, Reade GW, Roberts EPL (2009) Numerical modelling of a bromide-polysulphide redox flow battery. Part 2: evaluation of a utility-scale system. J Power Sources 189:1231–1239. doi:10.1016/j.jpowsour.2009.01.076
48. Sum E, Rychcik M, Skyllas-kazacos M (1985) Investigation of the V(V)/V(IV) system for use in the positive half-cell of a redox battery. J Power Sources 16:85–95. doi:10.1016/0378-7753(85)80082-3
49. Sum E, Skyllas-Kazacos M (1985) A study of the V(II)/V(III) redox couple for redox flow cell applications. J Power Sources 15:179–190. doi:10.1016/0378-7753(85)80071-9
50. Skyllas-Kazacos M, Rychcik M, Robins RG, Fane AG, Green MA (1986) New all-vanadium redox flow cell. J Electrochem Soc 133:1057–1058. doi:10.1149/1.2108706
51. Li B, Gu M, Nie Z, Shao Y, Luo Q, Wei X, Li X, Xiao J, Wang C, Sprenkle V, Wang W (2013) Bismuth nanoparticle decorating graphite felt as a high-performance electrode for an all-vanadium redox flow battery. Nano Lett 13:1330–1335. doi:10.1021/nl400223v
52. Li B, Gu M, Nie Z, Wei X, Wang C, Sprenkle V, Wang W (2014) Nanorod niobium oxide as powerful catalysts for an all vanadium redox flow battery. Nano Lett 14:158–165. doi:10.1021/nl403674a
53. Kazacos M, Cheng M, Skyllas-Kazacos M (1990) Vanadium redox cell electrolyte optimization studies. J Appl Electrochem 20:463–467. doi:10.1007/BF01076057
54. Li L, Kim S, Wang W, Vijayakumar M, Nie Z, Chen B, Zhang J, Xia G, Hu J, Graff G, Liu J, Yang Z (2011) A stable vanadium redox-flow battery with high energy density for large-scale energy storage. Adv Energy Mater 1:394–400. doi:10.1002/aenm.201100008
55. Kim S, Thomsen E, Xia G, Nie Z, Bao J, Recknagle K, Wang W, Viswanathan V, Luo Q, Wei X, Crawford A, Coffey G, Maupin G, Sprenkle V (2013) 1 kW/1 kWh advanced vanadium redox flow battery utilizing mixed acid electrolytes. J Power Sources 237:300–309. doi:10.1016/j.jpowsour.2013.02.045
56. Poizot P, Dolhem F (2011) Clean energy new deal for a sustainable world: from non-CO_2 generating energy sources to greener electrochemical storage devices. Energy Environ Sci 4:2003–2019. doi:10.1039/C0EE00731E
57. Huskinson B, Marshak MP, Suh C, Er S, Gerhardt MR, Galvin CJ, Chen X, Aspuru-Guzik A, Gordon RG, Aziz MJ (2014) A metal-free organic-inorganic aqueous flow battery. Nature 505:195–198. doi:10.1038/nature12909
58. Huskinson B, Marshak MP, Gerhardt MR, Aziz MJ (2014) Cycling of a quinone-bromide flow battery for large-scale electrochemical energy storage. ECS Trans 61:27–30. doi:10.1149/06137.0027ecst
59. Chambers JQ (1974) Electrochemistry of quinones. In: Patai S (ed) The chemistry of the quinonoid compounds Part 1, Chap. 14. Wiley, New York
60. Bailey SI, Ritchie IM (1985) A cyclic voltammetric study of the aqueous electrochemistry of some quinones. Electrochim Acta 30:3–12. doi:10.1016/0013-4686(85)80051-7
61. Huskinson B, Nawar S, Gerhardt MR, Aziz MJ (2013) Novel quinone-based couples for flow batteries. ECS Trans 53:101–105. doi:10.1149/05307.0101ecst
62. Xu Y, Wen Y-H, Cheng J, Cao G-P, Yang Y-S (2010) A study of tiron in aqueous solutions for redox flow battery application. Electrochim Acta 55:715–720. doi:10.1016/j.electacta.2009.09.031
63. Yang B, Hoober-Burkhardt L, Wang F, Prakash GKS, Narayanan SR (2014) An inexpensive aqueous flow battery for large-scale electrical energy storage based on water-soluble organic redox couples. J Electrochem Soc 161:A1371–A1380. doi:10.1149/2.1001409jes
64. Xu K (2004) Nonaqueous liquid electrolytes for lithium-based rechargeable batteries. Chem Rev 104:4303–4418. doi:10.1021/cr030203g
65. Cappillino PJ, Pratt HD, Hudak NS, Tomson NC, Anderson TM, Anstey MR (2014) Application of redox non-innocent ligands to non-aqueous flow battery electrolytes. Adv Energy Mater 4:n/a–n/a. doi:10.1002/aenm.201300566

66. Sleightholme AES, Shinkle AA, Liu Q, Li Y, Monroe CW, Thompson LT (2011) Non-aqueous manganese acetylacetonate electrolyte for redox flow batteries. J Power Sources 196:5742–5745. doi:10.1016/j.jpowsour.2011.02.020
67. Chakrabarti MH, Dryfe RAW, Roberts EPL (2007) Evaluation of electrolytes for redox flow battery applications. Electrochim Acta 52:2189–2195. doi:10.1016/j.electacta.2006.08.052
68. Zhang D, Lan H, Li Y (2012) The application of a non-aqueous bis(acetylacetone) ethylenediamine cobalt electrolyte in redox flow battery. J Power Sources 217:199–203. doi:10.1016/j.jpowsour.2012.06.038
69. Shinkle AA, Sleightholme AES, Griffith LD, Thompson LT, Monroe CW (2012) Degradation mechanisms in the non-aqueous vanadium acetylacetonate redox flow battery. J Power Sources 206:490–496. doi:10.1016/j.jpowsour.2010.12.096
70. Mun J, Lee M-J, Park J-W, Oh D-J, Lee D-Y, Doo S-G (2012) Non-aqueous redox flow batteries with nickel and iron tris(2,2′-bipyridine) complex electrolyte. Electrochem Solid-State Lett 15:A80–A82. doi:10.1149/2.033206esl
71. Matsuda Y, Tanaka K, Okada M, Takasu Y, Morita M, Matsumura-Inoue T (1988) A rechargeable redox battery utilizing ruthenium complexes with non-aqueous organic electrolyte. J Appl Electrochem 18:909–914. doi:10.1007/BF01016050
72. Chakrabarti MH, Roberts EPL, Bae C, Saleem M (2011) Ruthenium based redox flow battery for solar energy storage. Energy Convers Manage 52:2501–2508. doi:10.1016/j.enconman.2011.01.012
73. Liu Q, Sleightholme AES, Shinkle AA, Li Y, Thompson LT (2009) Non-aqueous vanadium acetylacetonate electrolyte for redox flow batteries. Electrochem Commun 11:2312–2315. doi:10.1016/j.elecom.2009.10.006
74. Liu Q, Shinkle AA, Li Y, Monroe CW, Thompson LT, Sleightholme AES (2010) Non-aqueous chromium acetylacetonate electrolyte for redox flow batteries. Electrochem Commun 12:1634–1637. doi:10.1016/j.elecom.2010.09.013
75. Shinkle AA, Sleightholme AES, Thompson LT, Monroe CW (2011) Electrode kinetics in non-aqueous vanadium acetylacetonate redox flow batteries. J Appl Electrochem 41:1191–1199. doi:10.1007/s10800-011-0314-z
76. Shinkle AA, Pomaville TJ, Sleightholme AES, Thompson LT, Monroe CW (2014) Solvents and supporting electrolytes for vanadium acetylacetonate flow batteries. J Power Sources 248:1299–1305. doi:10.1016/j.jpowsour.2013.10.034
77. Lee D-Y, Lee M-J, Park J-W, Oh D-J, Mun J-Y, Doo S-G (2011) Aromatic ligand coordinated redox couples & their application into redox flow batteries. The International Flow Battery Forum 2011 Edinburgh
78. Gagne RR, Koval CA, Lisensky GC (1980) Ferrocene as an internal standard for electrochemical measurements. Inorg Chem 19:2854–2855. doi:10.1021/ic50211a080
79. Wei X, Cosimbescu L, Xu W, Hu JZ, Vijayakumar M, Feng J, Hu MY, Deng X, Xiao J, Liu J, Sprenkle V, Wang W (2014) Towards high-performance nonaqueous redox flow electrolyte via ionic modification of active species. Adv Energy Mater n/a–n/a. doi:10.1002/aenm.201400678
80. Liang Y, Tao Z, Chen J (2012) Organic electrode materials for rechargeable lithium batteries. Adv Energy Mater 2:742–769. doi:10.1002/aenm.201100795
81. Song Z, Zhou H (2013) Towards sustainable and versatile energy storage devices: an overview of organic electrode materials. Energy Environ Sci 6:2280. doi:10.1039/c3ee40709h
82. Chen Z, Qin Y, Amine K (2009) Redox shuttles for safer lithium-ion batteries. Electrochim Acta 54:5605–5613. doi:10.1016/j.electacta.2009.05.017
83. Brushett FR, Vaughey JT, Jansen AN (2012) An all-organic non-aqueous lithium-ion redox flow battery. Adv Energy Mater 2:1390–1396. doi:10.1002/aenm.201200322
84. Zhang SS (2006) A review on electrolyte additives for lithium-ion batteries. J Power Sources 162:1379–1394. doi:10.1016/j.jpowsour.2006.07.074

85. Zhang L, Zhang Z, Redfern PC, Curtiss LA, Amine K (2012) Molecular engineering towards safer lithium-ion batteries: a highly stable and compatible redox shuttle for overcharge protection. Energy Environ Sci 5:8204–8207. doi:10.1039/C2EE21977H
86. Su L, Ferrandon M, Kowalski JA, Vaughey JT, Brushett FR (2014) Electrolyte development for non-aqueous redox flow batteries using a high-throughput screening platform. J Electrochem Soc 161:A1905–A1914. doi:10.1149/2.0811412jes
87. Wang W, Xu W, Cosimbescu L, Choi D, Li L, Yang Z (2012) Anthraquinone with tailored structure for a nonaqueous metal–organic redox flow battery. Chem Commun 48:6669–6671. doi:10.1039/C2CC32466K
88. Bachman JE, Curtiss LA, Assary RS (2014) Investigation of the redox chemistry of anthraquinone derivatives using density functional theory. J Phys Chem A. doi:10.1021/jp5060777
89. Hernández-Burgos K, Burkhardt SE, Rodríguez-Calero GG, Hennig RG, Abruña HD (2014) Theoretical studies of carbonyl-based organic molecules for energy storage applications: the heteroatom and substituent effect. J Phys Chem C 118:6046–6051. doi:10.1021/jp4117613
90. Hernández-Burgos K, Rodríguez-Calero GG, Zhou W, Burkhardt SE, Abruña HD (2013) Increasing the gravimetric energy density of organic based secondary battery cathodes using small radius cations (Li+ and Mg2+). J Am Chem Soc 135:14532–14535. doi:10.1021/ja407273c
91. Nishide H, Koshika K, Oyaizu K (2009) Environmentally benign batteries based on organic radical polymers. Pure Appl Chem 81:1961–1970. doi:10.1351/PAC-CON-08-12-03
92. Suga T, Nishide H (2011) Rechargeable batteries using robust but redox active organic radicals. In: Hicks R (ed) Stable radicals: fundamentals and applied aspects of odd-electron compounds, Chap. 14, 1st edn. Wiley, New York
93. Nakahara K, Iwasa S, Iriyama J, Morioka Y, Suguro M, Satoh M, Cairns EJ (2006) Electrochemical and spectroscopic measurements for stable nitroxyl radicals. Electrochim Acta 52:921–927. doi:10.1016/j.electacta.2006.06.028
94. Buhrmester C, Moshurchak LM, Wang RL, Dahn JR (2006) The use of 2,2,6,6-tetramethylpiperinyl-oxides and derivatives for redox shuttle additives in Li-ion cells. J Electrochem Soc 153:A1800–A1804. doi:10.1149/1.2221860
95. Li Z, Li S, Liu S, Huang K, Fang D, Wang F, Peng S (2011) Electrochemical properties of an all-organic redox flow battery using 2,2,6,6-tetramethyl-1-piperidinyloxy and N-methyl phthalimide. Electrochem Solid-State Lett 14:A171–A173. doi:10.1149/2.012112esl
96. Wei X, Xu W, Vijayakumar M, Cosimbescu L, Liu T, Sprenkle V, Wang W (2014) TEMPO-based catholyte for high-energy density nonaqueous redox flow batteries. Adv Mater 26:7649–7653. doi:10.1002/adma.201403746
97. Thaller L (1974) Electrically rechargeable redox flow cells. NASA-TM X-71540
98. Aaron DS, Liu Q, Tang Z, Grim GM, Papandrew AB, Turhan A, Zawodzinski TA, Mench MM (2012) Dramatic performance gains in vanadium redox flow batteries through modified cell architecture. J Power Sources 206:450–453. doi:10.1016/j.jpowsour.2011.12.026
99. Darling RM, Perry ML (2014) The influence of electrode and channel configurations on flow battery performance. J Electrochem Soc 161:A1381–A1387. doi:10.1149/2.0941409jes
100. Duduta M, Ho B, Wood VC, Limthongkul P, Brunini VE, Carter WC, Chiang Y-M (2011) Semi-solid lithium rechargeable flow battery. Adv Energy Mater 1:511–516. doi:10.1002/aenm.201100152
101. Li Z, Smith KC, Dong Y, Baram N, Fan FY, Xie J, Limthongkul P, Carter WC, Chiang Y-M (2013) Aqueous semi-solid flow cell: demonstration and analysis. Phys Chem Chem Phys 15:15833–15839. doi:10.1039/C3CP53428F
102. Fan FY, Woodford WH, Li Z, Baram N, Smith KC, Helal A, McKinley GH, Carter WC, Chiang Y-M (2014) Polysulfide flow batteries enabled by percolating nanoscale conductor networks. Nano Lett 14:2210–2218. doi:10.1021/nl500740t
103. Bradley CS (1885) Secondary battery. US Patent 312,802, 24 Feb 1885
104. Barnartt S, Forejt DA (1964) Bromine-zinc secondary cells. J Electrochem Soc 111:1201–1204. doi:10.1149/1.2425960

105. Lim HS, Lackner AM, Knechtli RC (1977) Zinc-bromine secondary battery. J Electrochem Soc 124:1154–1157. doi:10.1149/1.2133517
106. Pavlov D, Papazov G, Gerganska M (1991) Battery energy storage systems. The United Nations Educational, Scientific and Cultural Organization, Regional Office for Science and Technology for Europe, Technical Report No. 7
107. http://www.zbbenergy.com/products/flow-battery/. Accessed 30 Sept 2014
108. Adams GB (1979) Electrically rechargeable battery. US Patent 4,180,623, 25 Dec 1979
109. Magnani NJ, Clark RP, Braithwaite JW, Bush DM, Butler PC, Freese JM, Grothaus KR, Murphy KD, Shoemaker PE(1985) Exploratory battery technology development and testing report for 1985. Sandia National Laboratories
110. Clarke R, Dougherty B, Harrison S, Millington P, Mohanta S (2004) Cerium batteries. US Patent Application Publication 2004/0202925 A1, 14 Oct 2004
111. Clarke R, Dougherty B, Harrison S, Millington J, Mohanta S (2006) Battery with bifunctional electrolyte. US Patent Application Publication 2006/0063065 A1, 23 Mar 2006
112. Hazza A, Pletcher D, Wills R (2004) A novel flow battery: a lead acid battery based on an electrolyte with soluble lead(II) Part I. Preliminary studies. Phys Chem Chem Phys 6:1773. doi:10.1039/b401115e
113. Pletcher D, Wills R (2004) A novel flow battery: a lead acid battery based on an electrolyte with soluble lead(II) Part II. Flow cell studies. Phys Chem Chem Phys 6:1779–1785
114. Pletcher D, Wills R (2005) A novel flow battery: a lead acid battery based on an electrolyte with soluble lead(II) Part III. The influence of conditions on battery performance. J Power Sources 149:96–102. doi:10.1016/j.jpowsour.2005.01.048
115. Hazza A, Pletcher D, Wills R (2005) A novel flow battery: a lead acid battery based on an electrolyte with soluble lead(II) Part IV. The influence of additives. J Power Sources 149:103–111. doi:10.1016/j.jpowsour.2005.01.049
116. Pletcher D, Zhou H, Kear G, Low CTJ, Walsh FC, Wills RGA (2008) A novel flow battery: a lead-acid battery based on an electrolyte with soluble lead(II) Part V. Studies of the lead negative electrode. J Power Sources 180:621–629. doi:10.1016/j.jpowsour.2008.02.024
117. Pletcher D, Zhou H, Kear G, Low CTJ, Walsh FC, Wills RGA (2008) A novel flow battery: a lead-acid battery based on an electrolyte with soluble lead(II) Part VI. Studies of the lead dioxide positive electrode. J Power Sources 180:630–634. doi:10.1016/j.jpowsour.2008.02.025
118. Li X, Pletcher D, Walsh FC (2009) A novel flow battery: a lead acid battery based on an electrolyte with soluble lead(II) Part VII. Further studies of the lead dioxide positive electrode. Electrochim Acta 54:4688–4695. doi:10.1016/j.electacta.2009.03.075
119. Collins J, Kear G, Li X, Low CTJ, Pletcher D, Tangirala R, Stratton-Campbell D, Walsh FC, Zhang C (2010) A novel flow battery: a lead acid battery based on an electrolyte with soluble lead(II) Part VIII. The cycling of a 10 cm × 10 cm flow cell. J Power Sources 195:1731–1738. doi:10.1016/j.jpowsour.2009.09.044
120. Collins J, Li X, Pletcher D, Tangirala R, Stratton-Campbell D, Walsh FC, Zhang C (2010) A novel flow battery: a lead acid battery based on an electrolyte with soluble lead(II) Part IX: Electrode and electrolyte conditioning with hydrogen peroxide. J Power Sources 195:2975–2978. doi:10.1016/j.jpowsour.2009.10.109
121. Verde MG, Carroll KJ, Wang Z, Sathrum A, Meng YS (2013) Achieving high efficiency and cyclability in inexpensive soluble lead flow batteries. Energy Environ Sci 6:1573. doi:10.1039/c3ee40631h
122. Xu W, Wang J, Ding F, Chen X, Nasybulin E, Zhang Y, Zhang J-G (2014) Lithium metal anodes for rechargeable batteries. Energy Environ Sci 7:513–537. doi:10.1039/C3EE40795K
123. Tarascon J-M, Armand M (2001) Issues and challenges facing rechargeable lithium batteries. Nature 414:359–367. doi:10.1038/35104644
124. Christensen J, Albertus P, Sanchez-Carrera RS, Lohmann T, Kozinsky B, Liedtke R, Ahmed J, Kojic A (2011) A critical review of Li/air batteries. J Electrochem Soc 159:R1–R30. doi:10.1149/2.086202jes
125. Lu Y, Goodenough JB, Kim Y (2011) Aqueous cathode for next-generation alkali-ion batteries. J Am Chem Soc 133:5756–5759. doi:10.1021/ja201118f

126. Lu Y, Goodenough JB (2011) Rechargeable alkali-ion cathode-flow battery. J Mater Chem 21:10113–10117. doi:10.1039/C0JM04222F
127. Wang Y, He P, Zhou H (2012) Li-redox flow batteries based on hybrid electrolytes: at the cross road between Li-ion and redox flow batteries. Adv Energy Mater 2:770–779. doi:10.1002/aenm.201200100
128. Zhao Y, Byon HR (2013) High-performance lithium-iodine flow battery. Adv Energy Mater 3:1630–1635. doi:10.1002/aenm.201300627
129. Bruce PG, Freunberger SA, Hardwick LJ, Tarascon J-M (2012) Li–O_2 and Li–S batteries with high energy storage. Nat Mater 11:19–29. doi:10.1038/nmat3191
130. Su Y-S, Fu Y, Cochell T, Manthiram A (2013) A strategic approach to recharging lithium-sulphur batteries for long cycle life. Nat Commun. doi:10.1038/ncomms3985
131. Manthiram A, Fu Y, Chung S-H, Zu C, Su Y-S (2014) Rechargeable lithium–sulfur batteries. Chem Rev doi:10.1021/cr500062v
132. Rauh RD, Abraham KM, Pearson GF, Surprenant JK, Brummer SB (1979) A lithium/dissolved sulfur battery with an organic electrolyte. J Electrochem Soc 126:523–527. doi:10.1149/1.2129079
133. Manthiram A, Fu Y, Su Y-S (2013) Challenges and prospects of lithium–sulfur batteries. Acc Chem Res 46:1125–1134. doi:10.1021/ar300179v
134. Mikhaylik YV (2008) Electrolytes for lithium sulfur cells. US Patent 7,354,680 B2, 8 April 2008
135. Aurbach D, Pollak E, Elazari R, Salitra G, Kelley CS, Affinito J (2009) On the surface chemical aspects of very high energy density, rechargeable Li–sulfur batteries. J Electrochem Soc 156:A694–A702. doi:10.1149/1.3148721
136. Yang Y, Zheng G, Cui Y (2013) A membrane-free lithium/polysulfide semi-liquid battery for large-scale energy storage. Energy Environ Sci 6:1552–1558. doi:10.1039/C3EE00072A
137. Darling RM, Gallagher KG, Kowalski JA, Ha S, Brushett FR (2014) Pathways to low-cost electrochemical energy storage: a comparison of aqueous and nonaqueous flow batteries. Energy Environ Sci doi:10.1039/C4EE02158D